A CLASS OF MIXED ASSUMED STRAIN METHODS AND THE METHOD OF INCOMPATIBLE MODES*

'. . . two wrongs do make a right in California'   G. STRANG (1973)
'. . . two rights make a right even in California'   R. L. TAYLOR (1989)

J. C. SIMO† AND M. S. RIFAI‡

Division of Applied Mechanics, Department of Mechanical Engineering, Stanford University, Stanford, CA 94305, U.S.A.

SUMMARY

A three-field mixed formulation in terms of displacements, stresses and an *enhanced strain* field is presented which encompasses, as a particular case, the classical method of incompatible modes. Within this framework, incompatible elements arise as particular 'compatible' mixed approximations of the enhanced strain field. The conditions that the stress interpolation contain piece-wise constant functions and be L_2-orthogonal to the enhanced strain interpolation, ensure satisfaction of the patch test and allow the elimination of the stress field from the formulation. The preceding conditions are formulated in a form particularly convenient for element design. As an illustration of the methodology three new elements are developed and shown to exhibit good performance: a plane 3D elastic/plastic QUAD, an axisymmetric element and a thick plate bending QUAD. The formulation described herein is suitable for non-linear analysis.

1. INTRODUCTION AND MOTIVATION

In recent years, considerable attention has been devoted to the development of low order quadrilateral elements (typically bilinear) which exhibit *high accuracy in coarse meshes*, particularly in *bending dominated situations*. Furthermore, many of these low order elements do not exhibit the well-known 'spurious locking' in the nearly incompressible limit and are, therefore, particularly attractive in general purpose finite element analysis programs. It should be pointed out that, despite the enhanced accuracy of these quadrilaterals, from a numerical analysis standpoint no improvement on the standard (*asymptotic*) interpolation error estimates is typically obtained (see e.g. the analysis in Strang and Fix (Reference 20, p. 174)).

Broadly speaking, recent design and development of low order quadrilaterals with enhanced coarse mesh accuracy falls within the scope of two alternative approaches, referred to as *assumed strain* and *assumed stress* methods in what follows. Representative of the first approach is the pioneering work of Nagtegaal *et al.*[10] and Willan,[28] the related **B**-bar methods of Hughes[6] and Simo *et al.*,[19] and the mode-decomposition and Hu–Washizu methods of Belytschko and co-workers; see e.g. Belytschko and Bachrach,[4] among others. As noted in Simo and Hughes,[13] all of these assumed strain methods can be cast into a three-field variational framework, and

formulated as a **B**-bar method in which the discrete strain–displacement operator **B** of the standard displacement model is replaced by an *assumed strain* (**B**-bar) operator. On the other hand, assumed stress methods are based on a *two-field* variational formulation in which stresses and displacements are interpolated independently. Representative of this approach is the quadrilateral element of Pian and Sumihara[11] and Puch and Atluri.[12]

An alternative approach to the development of low order elements with enhanced performance in coarse meshes is the classical method of *incompatible modes*, originally introduced by Bazely *et al.*[3] in the context of plate bending problems and Wilson *et al.*[25] in the context of plane elasticity. In finite element textbooks, this class of methods is often presented as an example of either *'variational crimes'*[7,20] or 'useful tricks'.[26] We show that these methods arise merely as particular interpolations within a certain class of mixed methods described below. It is also interesting to note that recently proposed stress based mixed formulations, e.g. Pian and Sumihara,[11] exhibit essentially the same coarse mesh accuracy and distortion insensitivity as well-known modified incompatible mode elements; e.g. Taylor *et al.*[22]

The class of mixed assumed strain methods presented in this paper allows the systematic development of low order elements with enhanced accuracy for coarse meshes. Within the proposed three-field mixed finite element framework, the classical method of incompatible modes arises as a particular *conforming approximation* of the strain field. Furthermore, by exploiting this mixed finite element framework, one can improve on existing incompatible elements and design new elements. As concrete examples, we present a new element for elastoplastic stress analysis, a new axisymmetric element and a new plate bending element. Noteworthy features of the present approach are as follows.

1. Three simple conditions are proposed which guarantee satisfaction of the patch test and stability of the interpolation, and allow the complete elimination of the *independent* stress field from the finite element equations. Hence, the three-field formulation collapses to a two-field mixed method in terms of displacements and an assumed *enhanced strain* field.

2. The method of incompatible modes becomes simply a special instance of a *'conforming'* mixed method. The fact, often justified on physical grounds, that incompatible modes do not participate in the definition of the element traction and body force load vectors is a result of the variational structure of the method. Enhanced strain approximations derived from incompatible mode fields automatically satisfy the Taylor *et al.*[22] patch test condition.

3. The implementation of inelastic constitutive models; in particular, the classical *strain driven* return mapping algorithms of plasticity (see e.g. Simo and Hughes[14]) is the same as in standard displacement models. This situation is in sharp contrast with two-field *stress driven* mixed interpolations for which the return mappings take a substantially different format (see Simo *et al.*[18]).

4. The present approach can also be formulated as a **B**-bar method which satisfies the 'variational consistency condition' set forth in Simo and Hughes.[13] Such a condition, however, does not guarantee convergence. In fact, we show that the original incompatible element of Wilson *et al.*[25] can be formulated as a variationally consistent **B**-bar method which, as is well known, fails to converge for certain distorted meshes.

An outline of the paper is as follows. In Section 2 we introduce the proposed mixed approximation in the context of physically non-linear elasticity, and introduce the notion of *enhanced strain fields*. The straightforward extension of the methodology to incorporate plasticity is discussed in Appendix III. In Section 3 we address issues related to the convergence and stability of the method. In Section 4 we reformulate the two crucial conditions introduced in Section 2 as conditions on the strain field in the isoparametric space (sometimes referred to as *covariant*

strains). This reformulation is particularly convenient from an element design point of view. This point of view is illustrated with the development of two new elements for plane/3D and axisymmetric problems. To further illustrate the general applicability of the methodology, we consider in Section 5 its application to thick plates. As an example, a new plate bending element is developed. Numerical examples are presented in Section 6. As illustrated by a numerical simulation presented in this section, the proposed approach can be extended to geometrically non-linear problems. A detailed discussion, however, is deferred to a subsequent publication.

2. MODEL PROBLEM I: PHYSICALLY NON-LINEAR ELASTICITY

We introduce the proposed class of mixed assumed strain methods within the context of physically non-linear elasticity. As alluded to above, this class of mixed methods includes, as a particular case, the classical method of incompatible modes.

The central idea is as follows. We start with a *three-field* variational formulation of elasticity, and consider strain fields of the form

$$\boldsymbol{\varepsilon} = \underbrace{\nabla^s \mathbf{u}}_{\text{compatible}} + \underbrace{\tilde{\boldsymbol{\varepsilon}}}_{\text{enhanced}} \tag{1}$$

where $\nabla^s \mathbf{u}$ is the symmetric gradient of the displacement field. In a finite element context, we refer to $\tilde{\boldsymbol{\varepsilon}}$ as the *enhanced part* of the strain field. As discussed below, the finite element interpolation of the enhanced field $\tilde{\boldsymbol{\varepsilon}}$ is *not subject to any interelement continuity requirement* and, in particular, can be derived consistent with any given 'incompatible mode' field. We complete the formulation by eliminating the stress field via an orthogonality condition analogous to that considered in Simo and Hughes.[13] Two additional conditions on the mixed interpolations guarantee convergence and stability of the method, as discussed in detail in Section 3.

2.1. Three-field variational formulation of physically non-linear elasticity

Let $\mathcal{B} \subset \mathbb{R}^3$ be the domain occupied by an elastic body, with particles labelled by $\mathbf{x} \in \mathcal{B}$, displacement field $\mathbf{u} : \mathcal{B} \to \mathbb{R}^{n_{\text{dim}}}$, and stored energy function $W(\mathbf{x}, \boldsymbol{\varepsilon})$, where $\boldsymbol{\varepsilon}$ denotes the *infinitesimal* strain tensor. In addition, $\boldsymbol{\sigma}$ denotes the *actual* stress tensor and $1 \leqslant n_{\text{dim}} \leqslant 3$ is the spatial dimension of the problem. As usual, we assume that $W(\mathbf{x}, \bullet)$ is convex.

Further, let $\mathbf{u}$ be specified on a part $\partial_u \mathcal{B}$ of the boundary of $\mathcal{B}$ as $\bar{\mathbf{u}}$, and let the traction vector be specified on $\partial_\sigma \mathcal{B}$ as

$$\boldsymbol{\sigma} \hat{\mathbf{n}} = \bar{\mathbf{t}} \text{ (given)} \quad \text{on } \partial_\sigma \mathcal{B} \tag{2}$$

where $\hat{\mathbf{n}}$ is the normal field to $\partial_\sigma \mathcal{B}$. As usual, we assume that $\partial_u \mathcal{B}$ and $\partial_\sigma \mathcal{B}$ are disjoint with $\overline{\partial \mathcal{B}} = \overline{\partial_u \mathcal{B} \cup \partial_\sigma \mathcal{B}}$.

Now let V be the space of admissible displacement variations, defined in the standard fashion as

$$V := \{ \boldsymbol{\eta} \in [H^1(\mathcal{B})]^{n_{\text{dim}}} \,|\, \boldsymbol{\eta}|_{\partial_u \mathcal{B}} = \mathbf{0} \} \tag{3}$$

Further, we shall denote by $\mathcal{E}$ and S the spaces of admissible strain and stress variations, respectively. We have

$$\mathcal{E} = S = [L_2(\mathcal{B})]^{n_{\text{str}}} \tag{4}$$

For plane or three dimensional elasticity we have $n_{strs} = n_{dim} \times (n_{dim} + 1)/2$, whereas for axisymmetric problems $n_{dim} = 2$ and $n_{strs} = 4$. With this notation at hand, we consider the following three standard variational equations:

$$
\left.
\begin{array}{c}
\displaystyle\int_{\mathscr{B}} \nabla^s\boldsymbol{\eta} \cdot \boldsymbol{\sigma}\, \mathrm{d}V - G_{\mathrm{ext}}(\boldsymbol{\eta}) = 0 \\[2ex]
\displaystyle\int_{\mathscr{B}} \boldsymbol{\tau} \cdot [\nabla^s\boldsymbol{\eta} - \boldsymbol{\varepsilon}]\, \mathrm{d}V = 0 \\[2ex]
\displaystyle\int_{\mathscr{B}} \boldsymbol{\gamma} \cdot [- \boldsymbol{\sigma} + \partial_\varepsilon W(\mathbf{x}, \boldsymbol{\varepsilon})]\, \mathrm{d}V = 0
\end{array}
\right\}
\tag{5}
$$

for all variations $(\boldsymbol{\eta}, \boldsymbol{\gamma}, \boldsymbol{\tau}) \in V \times \mathscr{E} \times S$. Here $(\mathbf{u}, \boldsymbol{\varepsilon}, \boldsymbol{\sigma})$ denote the *actual* displacement strain and stress fields, respectively, and $G_{\mathrm{ext}}(\boldsymbol{\eta})$ is the virtual work of the external loading given by

$$
G_{\mathrm{ext}}(\boldsymbol{\eta}) := \int_{\mathscr{B}} \rho_0 \mathbf{b} \cdot \boldsymbol{\eta}\, \mathrm{d}V + \int_{\partial_\sigma\mathscr{B}} \bar{\mathbf{t}} \cdot \boldsymbol{\eta}\, \mathrm{d}\Gamma
\tag{6}
$$

Relations (5) are the Euler equations associated with the well-known Hu–Washizu principle for physically non-linear elasticity.

2.1.1. 'Enhanced' strain field, and modified variational formulation. Next, we introduce a reparametrization of the strain fields in the form given in (1). Consequently, any 'admissible strain variation' is also written as

$$
\boldsymbol{\gamma} = \underbrace{\nabla^s\boldsymbol{\eta}}_{\text{compatible}} + \underbrace{\tilde{\boldsymbol{\gamma}}}_{\text{enhanced}}; \quad \text{with} \quad \boldsymbol{\eta} \in V
\tag{7}
$$

The last variational equation $(5)_3$ then takes the form

$$
\int_{\mathscr{B}} \tilde{\boldsymbol{\gamma}} \cdot [- \boldsymbol{\sigma} + \partial_\varepsilon W(\mathbf{x}, \nabla^s\mathbf{u} + \tilde{\boldsymbol{\varepsilon}})]\, \mathrm{d}V
$$
$$
+ \int_{\mathscr{B}} \nabla^s\boldsymbol{\eta} \cdot [- \boldsymbol{\sigma} + \partial_\varepsilon W(\mathbf{x}, \nabla^s\mathbf{u} + \tilde{\boldsymbol{\varepsilon}})]\, \mathrm{d}V = 0
\tag{8}
$$

By substituting (1) into $(5)_2$, and combining $(5)_1$ and (8) we arrive at the following modified three-field variational problem:

$$
\boxed{
\begin{array}{c}
\displaystyle\int_{\mathscr{B}} \nabla^s\boldsymbol{\eta} \cdot \partial_\varepsilon W(\mathbf{x}, \nabla^s\mathbf{u} + \tilde{\boldsymbol{\varepsilon}})\, \mathrm{d}V - G_{\mathrm{ext}}(\boldsymbol{\eta}) = 0 \\[2ex]
\displaystyle\int_{\mathscr{B}} \boldsymbol{\tau} \cdot \tilde{\boldsymbol{\varepsilon}}\, \mathrm{d}V = 0 \\[2ex]
\displaystyle\int_{\mathscr{B}} \tilde{\boldsymbol{\gamma}} \cdot [- \boldsymbol{\sigma} + \partial_\varepsilon W(\mathbf{x}, \nabla^s\mathbf{u} + \tilde{\boldsymbol{\varepsilon}})]\, \mathrm{d}V = 0
\end{array}
}
\tag{9}
$$

for all variations $(\boldsymbol{\eta}, \tilde{\boldsymbol{\varepsilon}}, \boldsymbol{\tau}) \in V \times \tilde{\mathscr{E}} \times S$, with $\tilde{\mathscr{E}}$ being the space of enhanced strain fields.

Remarks 2.1.

1. Note that the local Euler–Lagrange equations associated with (9) are the standard equilibrium equations in $\mathscr{B}$; namely,

$$\left.\begin{aligned} \operatorname{div}\left[\partial_{\varepsilon} W(\mathbf{x}, \nabla^{s}\mathbf{u} + \tilde{\varepsilon})\right] + \rho_{0}\mathbf{b} &= \mathbf{0} \\ \tilde{\varepsilon} &= \mathbf{0} \\ \sigma &= \partial_{\varepsilon} W(\mathbf{x}, \nabla^{s}\mathbf{u} + \tilde{\varepsilon}) \end{aligned}\right\} \tag{10}$$

along with the stress boundary condition (2) on $\partial_{\sigma}\mathscr{B}$. Although $\tilde{\varepsilon} = \mathbf{0}$ in $\mathscr{B}$ for the continuum problem, in general $\tilde{\varepsilon}^{h} \neq \mathbf{0}$, when we introduce finite element approximations.

2. Equations (9)–(10) are the Euler equations of the functional

$$\Pi(\mathbf{u}, \tilde{\varepsilon}, \sigma) := \int_{\mathscr{B}}\left[W(\mathbf{x}, \nabla^{s}\mathbf{u} + \tilde{\varepsilon}) - \sigma\cdot\tilde{\varepsilon}\right]\mathrm{d}V - \int_{\mathscr{B}}\rho_{0}\mathbf{b}\cdot\mathbf{u}\,\mathrm{d}V - \int_{\partial_{\sigma}\mathscr{B}}\bar{\mathbf{t}}\cdot\mathbf{u}\,\mathrm{d}\Gamma \tag{11}$$

as a straightforward manipulation shows.

3. Observe that the space of *enhanced* strain fields is in $[L_{2}(\mathscr{B})]^{n_{\text{dim}}}$. Hence, *no interelement continuity on $\tilde{\varepsilon}$ need be enforced when constructing finite element approximations.* ∎

2.2. Mixed finite element approximations

Let $\mathscr{B} = \bigcup_{e=1}^{n_{\text{elm}}}\mathscr{B}_{e}$ be a finite element approximation constructed by means of standard *isoparametric* elements. Denoting by $\square = [-1, 1] \times \overset{n_{\text{dim}}}{\ldots} \times [-1, 1]$ the unit cube in isoparametric space, we thus have, for a typical element $\mathscr{B}_{e}$,

$$\xi \in \square \mapsto \mathbf{x}_{e} = \sum_{A=1}^{n_{\text{nodes}}^{e}} N^{A}(\xi)\mathbf{x}_{A} \in \mathscr{B}_{e} \tag{12}$$

where $N^{A}(\xi)$ $(A = 1, \ldots, n_{\text{nodes}}^{e})$ are the standard isoparametric shape functions satisfying

$$N^{A}(\xi_{B}) = \delta_{B}^{A} \tag{13}$$

and ξ_{B} $(B = 1, \ldots, n_{\text{nodes}}^{e})$ denote the vertices of $\square$. Using *vector notation* and standard conventions in finite element analysis (see e.g. Zienkiewicz and Taylor[27]) we write

$$\mathbf{u}_{e}^{h} = \mathbf{N}_{e}(\xi)\mathbf{d}_{e}, \quad \nabla^{s}\mathbf{u}_{e}^{h} = \mathbf{B}_{e}(\xi)\mathbf{d}_{e} \tag{14}$$

where $\mathbf{d}_{e} \in \mathbb{R}^{n_{\text{dim}} \times n_{\text{nodes}}}$ is the vector of element nodal displacements, and $\mathbf{B}_{e}(\xi)$ is the *discrete strain operator*.

2.2.1. The enhanced strain field interpolation.

We consider the following *discontinuous finite element* approximation for the space $\tilde{\mathscr{E}}$ of enhanced strain fields. Let $\chi_{e} : \mathscr{B}_{e} \to \mathbb{R}$ be the characteristic function of $\mathscr{B}_{e}$ defined as

$$\chi_{e} = \begin{cases} 1 & \text{iff } \mathbf{x} \in \mathscr{B}_{e} \\ 0 & \text{otherwise} \end{cases} \tag{15}$$

Then set

$$\boxed{\tilde{\mathscr{E}}^{h} := \left\{\tilde{\gamma}^{h} \in \tilde{\mathscr{E}} \,\middle|\, \tilde{\gamma}^{h} = \sum_{e=1}^{n_{\text{elm}}} \tilde{\gamma}_{e}(\xi)\chi_{e}, \text{ with } \tilde{\gamma}_{e}(\xi) = \mathbf{G}(\xi)\alpha_{e}, \text{ and } \alpha_{e} \in \mathbb{R}^{n_{\tilde{\varepsilon}}}\right\}} \tag{16}$$

Here, $\boldsymbol{\alpha}_e$ are $n_{\tilde{\xi}}$-local element strain parameters, and $\mathbf{G}(\xi)$ is a matrix of $\mathbb{R}^{n_{\sigma m}} \times \mathbb{R}^{n_{\tilde{\tau}}}$ prescribed functions with linearly independent columns, which define the enhanced strain interpolation. If the space $\tilde{\mathscr{E}}^h$ is to 'enhance' the standard strain field derived from the displacement approximation, it is natural to require that compatible strains of the form $(14)_2$ *are not* included in $\tilde{\mathscr{E}}^h$. More precisely, let

$$\nabla^s \mathscr{V}^h := \left\{ \gamma^h \in \mathscr{E} \,\bigg|\, \gamma^h = \sum_{e=1}^{n_{\text{elm}}} \gamma_e(\xi)\chi_e, \text{ with } \gamma_e(\xi) = \mathbf{B}(\xi)\mathbf{d}_e \right\} \tag{17}$$

denote the space of standard strain fields. Then we require

Condition (i). The enhanced strain interpolation $\tilde{\mathscr{E}}^h$ and the standard strain interpolation defined by $\nabla^s \mathscr{V}^h$ are *independent* in the sense that

$$\boxed{\tilde{\mathscr{E}}^h \cap \nabla^s \mathscr{V}^h = \varnothing} \tag{18}$$

In addition, we assume that the columns of $\mathbf{G}(\xi)$ are *linearly independent*.

Requirement (18) is the crucial condition which ensures *stability* of the enhanced strain approximation. In particular, as shown in Section 4, violation of (18) leads to a singular system of equations. The admissible choices of functions $\mathbf{G}(\xi)$ are intimately related to the structure of the approximating stress subspace S^h, as discussed below.

2.2.2. The assumed discrete stress field. We consider finite element stress fields $\tau^h \in S^h$ also *discontinuous* across element boundaries; i.e. of the form

$$\tau^h = \sum_{e=1}^{n_{\text{elm}}} \tau_e(\xi)\chi_e \tag{19}$$

where $\tau_e(\xi)$ is the assumed stress field over a typical element $\mathscr{B}_e$. We then eliminate the explicit appearance of the stress field in our finite element approximation by choosing S^h orthogonal to $\tilde{\mathscr{E}}^h$; i.e.

Condition (ii). S^h and $\tilde{\mathscr{E}}^h$ are L_2-*orthogonal*. Since any $(\tilde{\gamma}^h, \tau^h) \in \tilde{\mathscr{E}}^h \times S^h$ is discontinuous across element boundaries, (16) and (19) imply

$$\boxed{\langle \tau_e, \tilde{\gamma}_e \rangle_{L_2} := \int_{\mathscr{B}_e} \tilde{\gamma}_e(\xi) \cdot \tau_e(\xi) \, \mathrm{d}V = \boldsymbol{\alpha}_e \cdot \int_{\mathscr{B}_e} \mathbf{G}^{\mathrm{T}}(\xi)\tau_e(\xi) \, \mathrm{d}V = 0} \tag{20}$$

for any element $e = 1, 2, \ldots, n_{\text{elm}}$.

As a result of this condition, equation $(9)_2$ is identically satisfied, and the first term in $(9)_3$ vanishes. Hence, condition (ii) (above) effectively eliminates the stress field from the finite element equations. However, given an interpolation space $\tilde{\mathscr{E}}^h$ of enhanced strain fields, the orthogonality condition (ii) (above) may produce an overly constrained space S^h which would preclude convergence of the method. We prevent such a situation by requiring

Condition (iii). The space S^h of stress fields of the form (19) *must include at least piece-wise constant functions* after enforcing the orthogonality condition (20), i.e.

$$\tau^h = \sum_{e=1}^{n_{\text{elm}}} \tau_e^0 \chi_e \in S^h, \text{ with } \tau_e^0 = \text{constant} \tag{21}$$

We show below that, for linear elasticity, conditions (i) and (iii) imply satisfaction of the patch test in the sense of Taylor *et al.*[23] In fact, the original incompatible modes element of Wilson *et al.*[25] fails to satisfy condition (ii) when recast in the format of the present formulation (see Appendix I).

2.3. Finite element equations. Solution procedure

Substitution of the preceding interpolations into equations (9)$_1$ and (9)$_3$ yields the discrete non-linear system of equations

$$\left. \begin{array}{l} \displaystyle \mathop{\mathbf{A}}_{e=1}^{n_{\text{elm}}} \left[\mathbf{f}_e^{\text{int}}(\mathbf{d}_e, \boldsymbol{\alpha}_e) - \mathbf{f}_e^{\text{ext}} \right] = \mathbf{0} \\[12pt] \mathbf{h}_e(\mathbf{d}_e, \boldsymbol{\alpha}_e) = \mathbf{0}, \quad (e = 1, 2, \ldots, n_{\text{elm}}) \end{array} \right\} \tag{22}$$

where $\mathbf{A}$ denotes the standard assembly operator, and

$$\left. \begin{array}{l} \displaystyle \mathbf{f}_e^{\text{int}}(\mathbf{d}_e, \boldsymbol{\alpha}_e) := \int_{\mathscr{B}_e} \mathbf{B}^{\text{T}} \partial_\varepsilon W(\mathbf{x}, \mathbf{Bd}_e + \mathbf{G}\boldsymbol{\alpha}_e) \, \mathrm{d}V \\[12pt] \displaystyle \mathbf{h}_e(\mathbf{d}_e, \boldsymbol{\alpha}_e) := \int_{\mathscr{B}_e} \mathbf{G}^{\text{T}} \partial_\varepsilon W(\mathbf{x}, \mathbf{Bd}_e + \mathbf{G}\boldsymbol{\alpha}_e) \, \mathrm{d}V \end{array} \right\} \tag{23}$$

Observe that the *element external force vector* $\mathbf{f}_e^{\text{ext}}$ has the usual expression of the standard *displacement model*.

The solution of the system of equations can be easily accomplished by a Newton procedure that incorporates static condensation of the parameters $\boldsymbol{\alpha}_e$ at the element level. Let

$$\mathbf{C}^{(k)} := \partial_{\varepsilon\varepsilon}^2 W(\mathbf{x}, \mathbf{Bd}_e^{(k)} + \mathbf{G}\boldsymbol{\alpha}_e^{(k)}) \tag{24}$$

be the matrix of tangent elastic modulii associated with $(\mathbf{d}_e^{(k)}, \boldsymbol{\alpha}_e^{(k)})$, and set

$$\left. \begin{array}{l} \displaystyle \mathbf{H}_e^{(k)} := \int_{\mathscr{B}_e} \mathbf{G}^{\text{T}} \mathbf{C}^{(k)} \mathbf{G} \, \mathrm{d}V \\[12pt] \displaystyle \boldsymbol{\Gamma}_e^{(k)} := \int_{\mathscr{B}_e} \mathbf{G}^{\text{T}} \mathbf{C}^{(k)} \mathbf{B} \, \mathrm{d}V \end{array} \right\} \tag{25}$$

Then, the iteration proceeds as follows:

a. COMPUTE $\mathbf{h}_e^{(k)}$ by (23) and *update* at the element level $\boldsymbol{\alpha}_e^{(k)}$ by setting

$$\boldsymbol{\alpha}_e^{(k+1)} = \boldsymbol{\alpha}_e^{(k)} - [\mathbf{H}_e^{(k)}]^{-1} [\boldsymbol{\Gamma}_e^{(k)} \Delta \mathbf{d}_e^{(k)} - \mathbf{h}_e^{(k)}]$$

b. COMPUTE modified internal and tangent stiffness matrix by setting

$$
\left.
\begin{aligned}
\tilde{\mathbf{f}}_e^{\mathrm{int}^{(k)}} &= \mathbf{f}_e^{\mathrm{int}^{(k)}} - [\mathbf{H}_e^{(k)}]^{-1}\mathbf{h}_e^{(k)} \\
\tilde{\mathbf{k}}_e^{(k)} &= \int_{\mathscr{B}_e} \mathbf{B}^{\mathrm{T}}\mathbf{C}^{(k)}\mathbf{B}\,\mathrm{d}V - [\mathbf{\Gamma}_e^{(k)}]^{\mathrm{T}}[\mathbf{H}_e^{(k)}]^{-1}[\mathbf{\Gamma}_e^{(k)}]
\end{aligned}
\right\}
$$

c. ASSEMBLE and SOLVE for a new nodal displacement increment

$$
\left.
\begin{aligned}
\tilde{R}^{(k)} &:= \overset{n_{\mathrm{elm}}}{\underset{e=1}{\mathbf{A}}} [\mathbf{f}_e^{\mathrm{ext}} - \tilde{\mathbf{f}}_e^{\mathrm{int}}] \\
\tilde{\mathbf{K}}^{(k)} &:= \overset{n_{\mathrm{elm}}}{\underset{e=1}{\mathbf{A}}} \tilde{\mathbf{k}}_e^{(k)} \\
\Delta\mathbf{d}^{(k+1)} &:= [\tilde{\mathbf{K}}^{(k)}]^{-1}\,\tilde{R}^{(k)}
\end{aligned}
\right\}
$$

d. SET $\mathbf{d}^{(k+1)} = \mathbf{d}^{(k)} + \Delta\mathbf{d}^{(k+1)}$ and GOTO a.

Convergence of the preceding algorithm, obtained by straightforward linearization of equations (22)–(23), is attained when $\| \tilde{R}^{(k)} \| <$ TOL. *Observe that at least the parameters* $\alpha_e^{(k)}$ *and the element residuals* $\mathbf{h}_e^{(k)}$ *need to be stored at the element level.*

2.3.1. Extension to plasticity. The formulation presented above can be immediately extended to incorporate inelastic effects (e.g. plasticity and viscoplasticity) such that all the standard *strain driven return mapping algorithms for plasticity and viscoplasticity carry over without any modification* to the present mixed finite element context. This is in sharp contrast with stress based mixed finite element formulations where the structure of the conventional return maps is completely lost, and a different (more cumbersome) algorithmic treatment is necessary; see Simo *et al.*[18] As an illustration, the treatment of rate independent plasticity is presented in Appendix III. Numerical simulations for J_2-flow theory are presented in Section 6.

3. REMARKS ON CONVERGENCE AND STABILITY

In this section we examine convergence and stability conditions for the discrete problem emanating from the mixed formulation discussed in the preceding section. First, we show that condition (iii) above ensures satisfaction of the patch test and includes, in particular, the Taylor *et al.*[22] patch test requirement. To illustrate the role played by this additional *consistency* condition, we consider in Appendix I a detailed analysis of the original incompatible mode element of Wilson *et al.*[25] We explicitly show why this element does pass the patch test for certain distorted configurations, and give an explicit characterization of those stress fields for which the patch test is violated.

Next, we make use of an interpretation of the methodology developed above as a B-bar method, to show that condition (i) ensures a *unique* solution for the system of equations governing the discrete problem; hence the *stability* of the discrete problem. The fact that violation of (18) results in lack of uniqueness of the discrete problem is illustrated by means of a simple example. Throughout the present discussion, attention is restricted to *linear* elasticity so that $\mathbf{C} = $ constant in expression (24).

3.1. Consistency and the patch test

Since $\mathbf{C}$ is positive definite, the assumption of linear independence on the rows of $\mathbf{G}(\xi)$ is equivalent to the assumption that the matrix

$$\mathbf{H} := \int_\square \mathbf{G}^{\mathrm{T}}(\xi)\,\mathbf{C}\mathbf{G}(\xi)j(\xi)\,\mathrm{d}\xi \tag{26}$$

be *positive definite*; i.e.

$$\boxed{\boldsymbol{\alpha}_e^{\mathrm{T}}\mathbf{H}\boldsymbol{\alpha}_e > 0, \quad \text{for any } \boldsymbol{\alpha}_e \in \mathbb{R}^{n_\varepsilon}} \tag{27}$$

With this observation in mind, we examine the implications of conditions (ii) and (iii) on the structure of $\mathbf{G}(\xi)$ and their relation to the patch test. Let

$$\bar{\mathbf{G}} := \int_\square \mathbf{G}(\xi)j(\xi)\,\mathrm{d}\xi \tag{28}$$

where $j(\xi)$ is the Jacobian determinant of the isoparametric map. Choosing $\boldsymbol{\tau}_e^0 = \text{constant}$, for $e = 1, 2, \ldots, n_{\text{elm}}$, condition (ii) implies

$$\boldsymbol{\alpha}_e \cdot \bar{\mathbf{G}}^{\mathrm{T}}\boldsymbol{\tau}_e^0 = 0, \quad \forall\,\boldsymbol{\alpha}_e \in \mathbb{R}^{n_\varepsilon} \Rightarrow \bar{\mathbf{G}}^{\mathrm{T}}\boldsymbol{\tau}_e^0 = \mathbf{0} \tag{29}$$

Now, condition (iii) on S^h requires that *any* piece-wise constant stress be in S^h. Consequently, (29) must *hold for any* $\boldsymbol{\tau}_e^0 \in \mathbb{R}^{n_{\text{strn}}}$; and we have

$$\boxed{\bar{\mathbf{G}}^{\mathrm{T}}\boldsymbol{\tau}_e^0 = \mathbf{0}, \quad \forall\,\boldsymbol{\tau}_e^0 \in \mathbb{R}^{n_{\text{strn}}}} \tag{30}$$

We show that conditions (27) and (30) do, in fact, imply satisfaction of the patch test. In particular, (30) is satisfied if $\bar{\mathbf{G}} = 0$, a condition set forth in Taylor et al.[22]

3.1.1. The patch test.
Consider a nodal displacement vector $\mathbf{d}$, such that

$$\boldsymbol{\sigma}_e^0 := \mathbf{C}\mathbf{B}\mathbf{d}_e \equiv \text{constant} \tag{31}$$

for $e = 1, 2, \ldots, n_{\text{elm}}$. Then, equation $(22)_2$ gives

$$\begin{aligned}
\mathbf{h}_e &:= \int_\square \mathbf{G}^{\mathrm{T}}[\mathbf{C}\mathbf{B}\mathbf{d}_e]j(\xi)\,\mathrm{d}\xi + \mathbf{H}\boldsymbol{\alpha}_e \\
&= \bar{\mathbf{G}}^{\mathrm{T}}\boldsymbol{\sigma}_e^0 + \mathbf{H}\boldsymbol{\alpha}_e = \mathbf{0}
\end{aligned} \tag{32}$$

If (27) and (30) hold, then (32) gives $\boldsymbol{\alpha}_e = \mathbf{0}$ $(e = 1, 2, \ldots, n_{\text{elm}})$, and the internal force vector reduces to the standard displacement model, i.e.

$$\mathbf{f}_e^{\text{int}} = \left[\int_\square \mathbf{B}^{\mathrm{T}}\mathbf{C}\mathbf{B}j\,\mathrm{d}\xi\right]\mathbf{d}_e \tag{33}$$

which, by construction, satisfies the patch test. Hence, conditions (27) and (30) imply satisfaction of the patch test.

3.2. Stability of the discrete problem

We examine solvability and uniqueness of the solutions for the discrete finite element problem governed by the following system of $(n + m) \times (n + m)$ equations:

$$\begin{bmatrix} \mathbf{K} & \mathbf{\Gamma}^T \\ \mathbf{\Gamma} & \mathbf{H} \end{bmatrix} \begin{Bmatrix} \mathbf{d} \\ \mathbf{\alpha} \end{Bmatrix} = \begin{Bmatrix} \mathbf{F}^{\text{ext}} \\ \mathbf{0} \end{Bmatrix} \tag{34}$$

Here $n := n_{\text{nodes}} \times n_{\text{dim}} - n_{\text{bc}}$ and $m := n_{\text{elm}} \times n_{\xi}$, where n_{bc} is the number of nodal boundary conditions. Recall that, by assumption, $\mathbf{K}$ and $\mathbf{H}$ are *symmetric* and *positive definite*. The static condensation procedure of Section 2.3 then yields the reduced system

$$\bar{\mathbf{K}}\mathbf{d} = \mathbf{F}^{\text{ext}}$$
$$\bar{\mathbf{K}} := \mathbf{K} - \mathbf{\Gamma}^T\mathbf{H}^{-1}\mathbf{\Gamma} \tag{35}$$

Since $\mathbf{H}$ is invertible, if (35) has a unique solution, then $\mathbf{\alpha}$ are also uniquely defined by the expression $\mathbf{\alpha} = -\mathbf{H}^{-1}\mathbf{\Gamma}\mathbf{d}$. We show below that condition (18) ensures positive definiteness of the *reduced* stiffness matrix $\bar{\mathbf{K}}$; and hence uniqueness of solution for the symmetric system (35). The argument exploits the following interpretation of $\bar{\mathbf{K}}$.

3.2.1. Interpretation as a B-bar method.

The system of equations (34) can be formulated as a B-bar method in which the stiffness matrix $\bar{\mathbf{K}}$ is given by

$$\bar{\mathbf{K}} = \overset{n_{\text{elm}}}{\underset{e=1}{\mathbf{A}}} \int_{\mathscr{B}_e} \bar{\mathbf{B}}_e^T \mathbf{C} \bar{\mathbf{B}}_e \, dV \tag{36}$$

with $\bar{\mathbf{B}}$ defined by the expression

$$\bar{\mathbf{B}}_e(\xi) := \mathbf{B}_e(\xi) - \mathbf{G}_e(\xi)\mathbf{H}^{-1}\mathbf{\Gamma} \tag{37}$$

Furthermore, the B-bar method is variationally consistent in the sense that the following condition (set forth in Simo and Hughes[13]) holds:

$$\int_{\mathscr{B}_e} \bar{\mathbf{B}}_e^T \mathbf{C} [\mathbf{B}_e - \bar{\mathbf{B}}_e] \, dV = \mathbf{0} \tag{38}$$

The preceding result follows from a straightforward algebraic manipulation. First, substitution of the expression $\mathbf{\alpha}_e = -\mathbf{H}^{-1}\mathbf{\Gamma}\mathbf{d}_e$ into (1) defines, in view of (37), the total strain field as

$$\mathbf{\varepsilon}_e = \mathbf{B}_e\mathbf{d}_e + \mathbf{G}_e\mathbf{\alpha}_e = \bar{\mathbf{B}}_e\mathbf{d}_e \tag{39}$$

Consequently, the internal force vector in (23)$_1$ reduces to

$$\mathbf{f}_e^{\text{int}} = \int_{\mathscr{B}_e} \mathbf{B}_e^T \mathbf{C} [\mathbf{B}_e\mathbf{d}_e + \mathbf{G}_e\mathbf{\alpha}_e] \, dV = \left[\int_{\mathscr{B}_e} \mathbf{B}_e^T \mathbf{C} \bar{\mathbf{B}}_e \, dV \right] \mathbf{d}_e \tag{40}$$

A direct computation using definitions (25) then yields

$$\int_{\mathscr{B}_e} [\mathbf{B}_e - \bar{\mathbf{B}}_e]^T \mathbf{C} \bar{\mathbf{B}}_e \, dV = \mathbf{\Gamma}\mathbf{H}^{-1} \int_{\mathscr{B}_e} \mathbf{G}_e^T \mathbf{C} [\mathbf{B}_e - \mathbf{G}_e\mathbf{H}^{-1}\mathbf{\Gamma}] \, dV$$
$$= \mathbf{\Gamma}\mathbf{H}^{-1} [\mathbf{\Gamma} - \mathbf{H}\mathbf{H}^{-1}\mathbf{\Gamma}] = \mathbf{0} \tag{41}$$

which proves (38). Assembly of (40) and use of (38) yields (26).

It should be noted that *the fact that the scheme can be formulated as a variationally consistent* **B**-bar *method holds independent of condition* (*iii*) (equation (20)) or, equivalently, independent of condition (30), and *by no means implies convergence of the method*. In fact, as shown in Appendix I, the original incompatible mode element of Wilson *et al.*[25] furnishes an example of a **B**-bar method, which is variationally consistent and, nevertheless, fails to converge in general for distorted meshes.

3.2.2. Stability analysis. Let us denote by ker $[\mathbf{B}_e]$ and ker $[\bar{\mathbf{B}}_e]$ the null spaces of $\mathbf{B}_e$ and $\bar{\mathbf{B}}_e$, respectively. Recall that ker $[\mathbf{B}_e]$ consists of all the nodal infinitesimal rigid body variations; i.e. a vector $\mathbf{d}_e^{\mathrm{rig}}$ in ker $[\mathbf{B}_e]$ satisfies

$$\mathbf{B}_e \mathbf{d}_e^{\mathrm{rig}} = \mathbf{0} \Leftrightarrow \mathbf{d}_e^{\mathrm{rig}} = \text{nodal rigid body variation.} \tag{42a}$$

It is precisely this condition, along with the requirement that V^h does not contain rigid body variations, that renders the stiffness matrix $\mathbf{K}$ of the displacement method positive definite. Similarly, in view of (36), positive definiteness of $\bar{\mathbf{K}}$ holds if ker $[\bar{\mathbf{B}}_e]$ consists only of nodal infinitesimal rigid body variations; hence

$$\bar{\mathbf{K}} \text{ positive definite} \Leftrightarrow \text{ker} [\mathbf{B}_e] = \text{ker} [\bar{\mathbf{B}}_e] \tag{42b}$$

It is clear from expression (37) and the structure of Γ that if condition $\mathbf{B}_e \hat{\mathbf{d}}_e = \mathbf{0}$ holds, then condition $\bar{\mathbf{B}}_e \hat{\mathbf{d}}_e = \mathbf{0}$ also holds. Consequently, the inclusion ker $[\mathbf{B}_e] \subset$ ker $[\bar{\mathbf{B}}_e]$ always holds. We claim that the reverse inclusion holds if and only if condition (18) is satisfied; explicitly

$$\boxed{\text{ker} [\mathbf{B}_e] = \text{ker} [\bar{\mathbf{B}}_e] \Leftrightarrow \tilde{\mathscr{E}}^h \cap \nabla^s V^h = \varnothing} \tag{43}$$

To prove this claim we proceed in two steps, as follows:

(a) First, we prove that $\tilde{\mathscr{E}}^h \cap \nabla^s V^h \neq \varnothing$ implies that ker $[\mathbf{B}_e] \neq$ ker $[\bar{\mathbf{B}}_e]$. Assume that there is $\hat{\boldsymbol{\varepsilon}}^h \neq \mathbf{0}$ which is in $\tilde{\mathscr{E}}^h \cap \nabla^s V^h \neq \varnothing$. This implies that there are $\hat{\mathbf{d}}_e$ and $\hat{\boldsymbol{\alpha}}_e$ such that

$$\hat{\boldsymbol{\varepsilon}}^h = \mathbf{B}_e \hat{\mathbf{d}}_e = \mathbf{G}_e \hat{\boldsymbol{\alpha}}_e \neq \mathbf{0} \tag{44}$$

In particular, it follows that $\hat{\mathbf{d}}_e \notin$ ker $[\mathbf{B}_e]$. However, condition (44) along with the definitions of $\mathbf{H}$ and Γ imply that $\hat{\mathbf{d}}_e \in$ ker $[\bar{\mathbf{B}}_e]$, since

$$\bar{\mathbf{B}}_e \hat{\mathbf{d}}_e = \mathbf{B}\hat{\mathbf{d}}_e - \mathbf{G}_e \mathbf{H}^{-1} \int_{\mathscr{B}_e} \mathbf{G}_e^{\mathrm{T}} \mathbf{C} [\mathbf{B}_e \hat{\mathbf{d}}_e] \, \mathrm{d}V$$

$$= \mathbf{B}\hat{\mathbf{d}}_e - \mathbf{G}_e \mathbf{H}^{-1} \int_{\mathscr{B}_e} \mathbf{G}_e^{\mathrm{T}} \mathbf{C} [\mathbf{G}_e \hat{\boldsymbol{\alpha}}_e] \, \mathrm{d}V$$

$$= \mathbf{B}\hat{\mathbf{d}}_e - \mathbf{G}_e \mathbf{H}^{-1} \mathbf{H}\hat{\boldsymbol{\alpha}}_e = \mathbf{0} \tag{45}$$

Consequently, ker $[\mathbf{B}_e] \neq$ ker $[\bar{\mathbf{B}}_e]$.

(b) Conversely, we show that ker $[\mathbf{B}_e] \neq$ ker $[\bar{\mathbf{B}}_e]$ implies $\tilde{\mathscr{E}}^h \cap \nabla^s V^h \neq \varnothing$. In fact, suppose that there is $\hat{\mathbf{d}}_e \in$ ker $[\bar{\mathbf{B}}_e]$ such that $\hat{\mathbf{d}}_e \neq \mathbf{0}$ with $\hat{\mathbf{d}}_e \notin$ ker $[\mathbf{B}_e]$. Then, condition $\bar{\mathbf{B}}_e \hat{\mathbf{d}}_e = \mathbf{0}$ and expression (37) imply that

$$\hat{\boldsymbol{\varepsilon}}^h := \mathbf{B}_e \hat{\mathbf{d}}_e = \mathbf{G}_e [\mathbf{H}^{-1} \Gamma \hat{\mathbf{d}}_e] \neq \mathbf{0} \tag{46}$$

Setting $\hat{\boldsymbol{\alpha}}_e = \mathbf{H}^{-1} \Gamma \hat{\mathbf{d}}_e$, equation (46) implies that $\hat{\boldsymbol{\varepsilon}}^h \in \tilde{\mathscr{E}}^h \cap \nabla^s V^h \neq \varnothing$. ∎

To summarize our stability analysis, since $\mathbf{K}$ is positive definite, the results above show that the system (34) (or the reduced system (35)) is uniquely solvable if and only if the following conditions hold:

(i) $\mathbf{H}$ is *positive definite*; equivalently, the columns of $\mathbf{G}$ are linearly independent.
(ii) $\tilde{\mathscr{E}}^h \cap \nabla^s V^h = \varnothing$; equivalently, the enhanced strains (generated by $\mathbf{G}$) are independent of the standard strain field generated by the displacement approximation.

The simple example below illustrates a choice of interpolation functions $\mathbf{G}(\xi)$ for which conditions (ii) and (iii) of Section 2 are satisfied, but the stability condition (i) of Section 2 is violated, leading to an unstable formulation. In fact, the example yields the one-point uniformly reduced bilinear quadrilateral which is rank deficient.

Example 3.1. Consider a square bilinear element with bi-unit sides, so that no distinction needs to be made between Cartesian and isoparametric co-ordinates. Further, consider the following interpolation (restricted for simplicity to square elements):

$$\mathbf{G}(\xi) = \begin{bmatrix} \eta & 0 & 0 & 0 \\ 0 & \xi & 0 & 0 \\ 0 & 0 & \xi & \eta \end{bmatrix} \tag{47}$$

A straightforward calculation shows that $\bar{\mathbf{B}}_e$ is constant and given by $\bar{\mathbf{B}}_e = \mathbf{B}_e(\xi)|_{\xi = 0}$. Clearly, the stiffness matrix $\bar{\mathbf{K}}$ is that associated with the one-point uniformly reduced integration element which is rank deficient, and the method is unstable. Observe that for the square element, the standard strain field $\nabla^s \mathbf{\eta}^h$ associated with any $\mathbf{\eta} \in V^h$ is of the form

$$\nabla^s \mathbf{\eta}^h \in \text{span} \begin{bmatrix} 1 & 0 & 0 & \eta & 0 & 0 & 0 \\ 0 & 1 & 0 & 0 & \xi & 0 & 0 \\ 0 & 0 & 1 & 0 & 0 & \xi & \eta \end{bmatrix} \tag{48}$$

which contains functions in the span of (47). Consequently, $\tilde{\mathscr{E}}^h \cap \nabla^s V^h \neq \varnothing$ and condition (i) of Section 2 is violated.   ■

3.3. Stress recovery

It is apparent from the basic equations (22)–(23) that the stress field $\mathbf{\sigma}^h \in S^h$ does not enter explicitly in the determination of the nodal displacements $\mathbf{d} \in \mathbb{R}^{n_{\text{dim}} \times n_{\text{nodes}}}$, and the enhanced strain parameters $\mathbf{\alpha} \in \mathbb{R}^{n_{\text{elm}} \times n_i}$. A variationally consistent recovery of the stress field from the nodal displacements $\mathbf{d}$ which, remarkably, does not involve the enhanced strain field, proceeds as follows.

3.3.1. Least-squares variational recovery.
Assume that the *displacement field u is given* and consider, for simplicity, linear elasticity so that the elasticity tensor $\mathbf{C} = $ constant. Consider the following least-square functional:

$$L(\tilde{\mathbf{\epsilon}}, \mathbf{\sigma}) := \int_{\mathscr{B}} [\mathbf{C}(\nabla^s \mathbf{u} + \tilde{\mathbf{\epsilon}}) - \mathbf{\sigma}] \cdot \mathbf{C}^{-1} [\mathbf{C}(\nabla^s \mathbf{u} + \tilde{\mathbf{\epsilon}}) - \mathbf{\sigma}] \, dV \tag{49}$$

where $(\tilde{\mathbf{\epsilon}}, \mathbf{\sigma}) \in \tilde{\mathscr{E}} \times S$ and $\mathbf{u}$ is regarded as fixed. We claim that the least-squares minimization

problem

$$L(\tilde{\boldsymbol{\varepsilon}}^h, \boldsymbol{\sigma}^h) = \underset{(\tilde{\gamma}^h, \boldsymbol{\tau}^h) \in \tilde{\mathscr{E}}^h \times S^h}{\text{MIN}} [L(\tilde{\gamma}^h, \boldsymbol{\tau}^h)] \tag{50}$$

defines the enhanced strain and stress fields $(\tilde{\boldsymbol{\varepsilon}}^h, \boldsymbol{\sigma}^h) \in \tilde{\mathscr{E}}^h \times S^h$. To see this, observe that the first variation of $L(\tilde{\boldsymbol{\varepsilon}}, \boldsymbol{\sigma})$ yields the variational equations

$$\left.\begin{array}{l} \displaystyle\int_{\mathscr{B}} \tilde{\gamma}^h \cdot \mathbf{C}\left[\nabla^s \mathbf{u}^h + \tilde{\boldsymbol{\varepsilon}}^h\right] \mathrm{d}V = 0 \\[10pt] \displaystyle\int_{\mathscr{B}} \boldsymbol{\tau}^h \cdot \left[\mathbf{C}^{-1}\boldsymbol{\sigma}^h - \nabla^s \mathbf{u}^h\right] \mathrm{d}V = 0 \end{array}\right\} \tag{51}$$

for all $(\tilde{\gamma}^h, \boldsymbol{\tau}^h) \in \tilde{\mathscr{E}}^h \times S^h$, where we have made use of the orthogonality condition (20). Substitution into (51) of the interpolations (14) and (16) for displacement and enhanced strain fields, respectively, yields (34)$_2$ which is the linear version of equations (22)$_2$ and gives, therefore, the correct values of the enhanced strain parameters $\boldsymbol{\alpha}_e$. The new information leading to the recovery of the stress field $\boldsymbol{\sigma}^h \in S^h$ is provided by (51)$_1$.

3.3.2. Stress recovery.

We consider a *subspace* $S_0^h \subset S^h$ of the admissible stresses defined as

$$S_0^h = \{\boldsymbol{\tau}^h \in S^h \mid \boldsymbol{\tau}^h = \boldsymbol{\tau}_e(\boldsymbol{\xi})\chi_e \text{ with } \boldsymbol{\tau}_e(\boldsymbol{\xi}) = \mathbf{G}_\sigma(\boldsymbol{\xi})\boldsymbol{\eta}_e\} \tag{52}$$

Here, $\mathbf{G}_\sigma(\boldsymbol{\xi})$ is a matrix of functions whose n_σ columns are linearly independent, and such that S_0^h satisfies conditions (i), (ii) and (iii) above. Substitution of (52) into (51) yields the *optimal* stress field (in a least-square sense) in S_0^h as

$$\left.\begin{array}{l} \boldsymbol{\sigma}_e(\boldsymbol{\xi}) = \mathbf{G}_\sigma(\boldsymbol{\xi})\mathbf{H}_\sigma^{-1}\boldsymbol{\Gamma}_\sigma \mathbf{d}_e \\[10pt] \mathbf{H}_\sigma := \displaystyle\int_{\mathscr{B}_e} \mathbf{G}_\sigma^{\mathrm{T}}(\boldsymbol{\xi})\mathbf{C}^{-1}\mathbf{G}_\sigma(\boldsymbol{\xi})\,\mathrm{d}V \\[10pt] \boldsymbol{\Gamma}_\sigma := \displaystyle\int_{\mathscr{B}_e} \mathbf{G}_\sigma^{\mathrm{T}}(\boldsymbol{\xi})\mathbf{B}(\boldsymbol{\xi})\,\mathrm{d}V \end{array}\right\} \tag{53}$$

for all elements $e = 1, 2, \ldots, n_{\text{elm}}$.

Remark 3.2. In particular, for $S_0^h = $ piece-wise constant functions, expression (53) yields

$$\boxed{\boldsymbol{\sigma}_0^h = \mathbf{C}\frac{1}{\text{Vol}(\mathscr{B}_e)}\left[\int_{\mathscr{B}_e} \mathbf{B}\,\mathrm{d}V\right]\mathbf{d}_e} \tag{54}$$

For Cartesian problems (as opposed to axisymmetry), expression (46) boils down to evaluation of the stresses at the centre of the element. ∎

4. ELEMENT DESIGN: ENHANCED STRAIN FIELD INTERPOLATION

In this section we consider the reformulation of conditions (ii) and (iii) of Section 2.2.2 above in a form which leads to a systematic construction of interpolation functions $\mathbf{G}(\boldsymbol{\xi})$.

The idea is to operate in the isoparametric domain in place of the physical domain and transform the results appropriately with the Jacobian of the isoparametric map at the centre of the element. We give two illustrative and representative examples: a plane elasticity element that

improves upon the element of Taylor *et al.*,[22] and the axisymmetry version of this element. A new plate bending element is developed in Section 5.

4.1. Reformulation of conditions on the assumed strain and stress fields

We shall denote by $x = \varphi(\xi)$ the isoparametric map, and think of it as a deformation $\varphi: \square \rightarrow \mathscr{B}_e$ (see Figure 1) with associated deformation gradient and Jacobian determinant

$$\mathbf{J}(\xi) := \frac{\partial \varphi}{\partial \xi}(\xi); \quad j(\xi) := \det[\mathbf{J}(\xi)] \tag{55}$$

respectively. The *constant deformation gradient* and *constant Jacobian*, obtained by evaluation of (55) at $\xi = \mathbf{0}$, are denoted by

$$\mathbf{J}_0 = \mathbf{J}(\xi)|_{\xi = 0}, \quad \text{and} \quad j_0 = j(\xi)|_{\xi = 0} \tag{56}$$

The idea now is to define the stress and enhanced strain fields $(\sigma, \tilde{\varepsilon})$ in physical space, in terms of objects $(\Sigma, \tilde{E})$ defined in the isoparametric space, as follows.

4.1.1. Transformation rules. Tensor and vector notation. As rank two tensors, we set

$$\boxed{\begin{aligned} \Sigma_{AB} &:= (J_0^{-1})_{Ai}\sigma_{ij}(J_0^{-1})_{Bj} \\ \tilde{E}_{AB} &:= \frac{j}{j_0} J_{0iA} \tilde{\varepsilon}_{ij} J_{0jB} \end{aligned}} \tag{57*}$$

Thus, given $(\Sigma_{AB}, \tilde{E}_{AB})$ in isoparametric space, the stress and enhanced strain $(\sigma_{ij}, \tilde{\varepsilon}_{ij})$ in physical space are obtained by convecting $(\Sigma_{AB}, \tilde{E}_{AB})$ with the Jacobian of the isoparametric map according to the standard rules (57)* of tensor calculus.

The counterpart of relations (57)* for the case of interest in which $(\sigma, \tilde{\varepsilon})$ and $(\Sigma, \tilde{E})$ are given in the usual finite element vector notation can be expressed as

$$\boxed{\Sigma(\xi) = \mathbf{F}_0^{-1}\sigma(\xi) \quad \text{and} \quad \tilde{E}(\xi) = \frac{j(\xi)}{j_0}\mathbf{F}_0^T\tilde{\varepsilon}(\xi)} \tag{57}$$
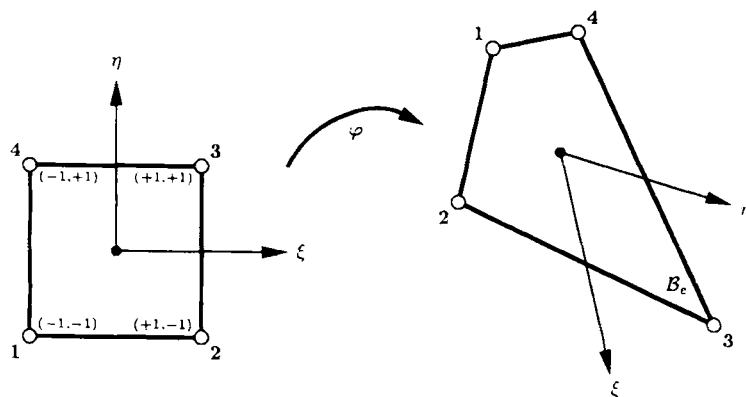
Figure 1. The isoparametric map $x = \varphi(\xi)$ as a map $\varphi: \square \rightarrow \mathscr{B}_e$

Here Σ, $\tilde{E}$, σ, $\tilde{\varepsilon}$ are vectors in $\mathbb{R}^{n_{\text{strs}}}$ and $\mathbf{F}_0$ is an $(n_{\text{strs}} \times n_{\text{strs}})$ matrix. (Recall that $n_{\text{strs}} = n_{\text{dim}} \times (n_{\text{dim}} + 1)/2$ for Cartesian problems, whereas $n_{\text{dim}} = 2$ and $n_{\text{strs}} = 4$ for axisymmetric problems.)

Example 4.1. For plane elasticity $n_{\text{dim}} = 2$, $n_{\text{strs}} = 3$, and we set

$$\sigma = [\sigma_{11} \quad \sigma_{22} \quad \sigma_{12}]^{\text{T}}, \quad \tilde{\varepsilon} = [\tilde{\varepsilon}_{11} \quad \tilde{\varepsilon}_{22} \quad 2\tilde{\varepsilon}_{12}]^{\text{T}}$$

$$\Sigma = [\Sigma_{11} \quad \Sigma_{22} \quad \Sigma_{12}]^{\text{T}}, \quad \tilde{E} = [\tilde{E}_{11} \quad \tilde{E}_{22} \quad 2\tilde{E}_{12}]^{\text{T}}$$

(58)

$\mathbf{F}_0$ is then the 3×3 matrix given by

$$\mathbf{F}_0 := \begin{bmatrix} J_{11}^2 & J_{21}J_{12} & 2J_{11}J_{12} \\ J_{12}J_{21} & J_{22}^2 & 2J_{21}J_{22} \\ J_{11}J_{21} & J_{12}J_{22} & (J_{11}J_{22} + J_{12}J_{21}) \end{bmatrix}_{\xi = 0}$$

(59)

where $J_{\alpha\beta} = \partial\varphi_\alpha/\partial\xi_\beta$.   ■

4.1.2. Construction of enhanced strain interpolations. As alluded to above, we shall always regard the interpolations of $\tilde{E}$ in isoparametric space as the primary variables, and then transform these interpolations via formulae (57). Accordingly, we adopt the following point of view (rather convenient in element design).

(i) Define the interpolation functions $\mathbf{E}(\xi)$ for the enhanced strain field $\tilde{E}(\xi)$ in isoparametric space; e.g.

$$\tilde{E}_e = \mathbf{E}(\xi)\alpha_e, \quad \alpha_e \in \mathbb{R}^{n_\varepsilon}$$

(60)

where $n_\varepsilon \geqslant n_{\text{strs}}$.

(ii) Obtain the interpolation functions $\mathbf{G}(\xi)$ for the enhanced strain field $\tilde{\varepsilon}(\xi)$ in physical space via formulae (57); i.e.

$$\mathbf{G}(\xi) := \frac{j_0}{j(\xi)} \mathbf{F}_0^{-\text{T}} \mathbf{E}(\xi)$$

(61)

The only design condition imposed on the functions $\mathbf{E}(\xi)$ emanates from (30), and in view of (28) and (61) now takes the simple form (recall that j_0 and $\mathbf{F}_0^{-\text{T}}$ are constant)

$$\int_\square \mathbf{E}(\xi)\,d\xi = 0$$

(62)

Requirement (62) and expression (61) guarantee that the approximating subspace contains piece-wise constant stresses (condition (iii) in Section 2.2.2) and hence insure satisfaction of the patch test. Finally, the orthogonality condition (20) now takes the form

$$\langle \tau_e, \tilde{\gamma}_e \rangle_{L_2} = \int_\square \frac{j_0}{j(\xi)} \mathbf{F}_0^{-\text{T}} \tilde{E}(\xi) \cdot \mathbf{F}_0 \Sigma(\xi) j(\xi)\,d\xi$$

$$= \int_\square \tilde{E}(\xi) \cdot \Sigma(\xi)\,d\xi$$

(63)

Remarks 4.1.

1. The interpolation functions $\mathbf{G}(\xi)$ obtained via (61) *are automatically frame invariant* provided, of course, that $\mathbf{E}(\xi)$ is $\{\xi, \eta\}$-invariant.
2. Often, one defines an interpolation space S^h by giving the form of the interpolations for $\Sigma(\xi)$. Then, one determines $\mathbf{E}(\xi)$ by exploiting conditions (62) and (63). Examples that illustrate this construction are given below.
3. The strain field $\tilde{E}$ can be defined from an 'incompatible' displacement field as follows. Let the incompatible field be denoted by $\tilde{\mathbf{u}}(\xi)$. Then, the components $\tilde{E}_{\alpha\beta}(\xi)$ of the enhanced strain field in isoparametric space are

$$\tilde{E}_{\alpha\beta}(\xi) = \frac{1}{2}\left[\frac{\partial\tilde{\mathbf{u}}(\xi)}{\partial\xi_\beta}\cdot\frac{\partial\varphi(\xi)}{\partial\xi_\alpha} + \frac{\partial\tilde{\mathbf{u}}(\xi)}{\partial\xi_\alpha}\cdot\frac{\partial\varphi(\xi)}{\partial\xi_\beta}\right] \tag{64}$$

See Appendix II for a concrete example.   ∎

4.2. Example 1: A plane elasticity (incompatible mode-like) element

We start with the standard four-node bilinear isoparametric element, and construct a five-parameter interpolation for the enhanced strain field according to the steps in Section 4.1.2 as follows.

4.2.1. The initial enhanced strain field.
We start with an enhanced strain field in isoparametric space which is derived from the original Wilson et al.[25] incompatible modes. It can be shown (see Appendix II) that such a field is given in terms of six parameters by the following interpolations:

$$\mathbf{E}_w(\xi) = \begin{bmatrix} \xi & 0 & 0 & 0 & \xi\eta & 0 \\ 0 & \eta & 0 & 0 & 0 & \xi\eta \\ 0 & 0 & \xi & \eta & \xi^2 & \eta^2 \end{bmatrix} \tag{65}$$

Clearly, $\mathbf{E}_w(\xi)$ *does not* satisfy condition (62); in fact

$$\int_\square \mathbf{E}_w(\xi)\,\mathrm{d}\xi = \begin{bmatrix} \mathbf{0}_{3\times4} & \begin{vmatrix} 0 & 0 \\ 0 & 0 \\ \frac{4}{3} & \frac{4}{3} \end{vmatrix} \end{bmatrix} \neq \mathbf{0} \tag{66}$$

We derive an interpolation matrix $\mathbf{E}(\xi)$ satisfying (62) by enforcing the orthogonality condition (63).

4.2.2. Assumed stress field: Orthogonality condition.
We consider discontinuous stress fields of the form (19) with $\tau_e(\xi)$ defined by the transformation rule $(57)_1$ and

$$\Sigma(\xi) = \begin{bmatrix} 1 & 0 & 0 & \eta & 0 \\ 0 & 1 & 0 & 0 & \xi \\ 0 & 0 & 1 & 0 & 0 \end{bmatrix}\beta; \quad \beta \in \mathbb{R}^5 \tag{67}$$

Let $\tilde{E}(\xi) = \mathbf{E}_w(\xi)\alpha$, $\alpha \in \mathbb{R}^6$. Enforcing the orthogonality condition (63) we conclude that

$$\alpha_5 = -\alpha_6 \tag{68}$$

Consequently, we arrive at the interpolation matrix

$$\mathbf{E}(\xi) = \begin{bmatrix} \xi & 0 & 0 & 0 & \xi\eta \\ 0 & \eta & 0 & 0 & -\xi\eta \\ 0 & 0 & \xi & \eta & \xi^2 - \eta^2 \end{bmatrix} \tag{69}$$

Note that, by construction, $\mathbf{E}(\xi)$ satisfies condition (62). The final set $\mathbf{G}(\xi)$ of interpolation functions is now obtained via the transformation (61). The performance of this element is slightly superior to that of Taylor et al.;[22] see Section 6.

Remark 4.2. Consider the interpolation field $\mathbf{E}_t(\xi)$ obtained by deleting the last column in (69); i.e.

$$\mathbf{E}_t(\xi) = \begin{bmatrix} \xi & 0 & 0 & 0 \\ 0 & \eta & 0 & 0 \\ 0 & 0 & \xi & \eta \end{bmatrix} \tag{70}$$

It can be easily shown that the interpolation functions

$$\mathbf{G}_t(\xi) := \frac{j_0}{j(\xi)} \mathbf{F}_0^{-\mathrm{T}} \mathbf{E}_t(\xi) \tag{71}$$

are in fact *identical* to the modified incompatible mode approximation of Taylor et al.[22] which, in contrast with the Wilson et al.[25] original formulation, is designed to satisfy the patch test (Strang's celebrated quote, 'Two wrongs do make a right in California'[20]). ∎

4.3. Example 2: Axisymmetric element

We consider the generalization of the interpolation developed in the preceding example to the axisymmetric case. We consider first the counterpart in the axisymmetric case of the interpolation in Remark 4.2 which is consistent with the incompatible mode approximation of Taylor et al.[22] In contrast with the plane (or 3D) problem, we show that in the axisymmetric case, the resulting enhanced strain interpolation is *no longer consistent with an incompatible displacement field*. The extension of these results to the interpolation in (69) is immediate.

4.3.1. Notation for axisymmetry. We consider a polar axisymmetric co-ordinate system $\{r, \theta, z\}$, with z along the axis of symmetry, and use the following vector notation for the stress and strain fields:

$$\begin{aligned} \boldsymbol{\sigma} &= [\sigma_{rr} \quad \sigma_{zz} \quad \sigma_{rz} \quad \sigma_{\theta\theta}]^{\mathrm{T}}, \quad \tilde{\boldsymbol{\varepsilon}} = [\tilde{\varepsilon}_{rr} \quad \tilde{\varepsilon}_{zz} \quad 2\tilde{\varepsilon}_{rz} \quad \tilde{\varepsilon}_{\theta\theta}]^{\mathrm{T}} \\ \boldsymbol{\Sigma} &= [\Sigma_{rr} \quad \Sigma_{zz} \quad \Sigma_{rz} \quad \Sigma_{\theta\theta}]^{\mathrm{T}}, \quad \tilde{\boldsymbol{E}} = [\tilde{E}_{11} \quad \tilde{E}_{22} \quad 2\tilde{E}_{12} \quad \tilde{E}_{\theta\theta}]^{\mathrm{T}} \end{aligned} \tag{72}$$

Further, we recall that the volume element (per unit radiant) can be written in the following form:

$$\frac{1}{2\pi} \mathrm{d}V = r(\xi)\,\mathrm{d}r\,\mathrm{d}z = r(\xi)j(\xi)\,\mathrm{d}\xi \tag{73}$$

where, as in the plane case, $\mathrm{d}\xi = \mathrm{d}\xi\,\mathrm{d}\eta$ and $\square = [-1, 1] \times [-1, 1]$. Here $j(\xi)$ denotes the determinant of the Jacobian associated with the isoparametric map, and is given by identical

expression as in the plane case; see (A3) and (A7) of Appendix I. In addition, in accordance with the notation of Appendix I, we set

$$r = \mathbf{r}^T \mathbf{N}(\xi), \quad z = \mathbf{z}^T \mathbf{N}(\xi)$$

$$\mathbf{r} = [r_1 \quad r_2 \quad r_3 \quad r_4]^T \tag{74}$$

$$\mathbf{z} = [z_1 \quad z_2 \quad z_3 \quad z_4]^T$$

where (r_A, z_A), $A = 1, \ldots, 4$ are the co-ordinates of the nodal points of a typical element $\mathscr{B}_e$, and $\mathbf{N}(\xi)$ is given by (A1).

4.3.2. Enhanced strain field interpolation. Motivated by the arguments in Remark 4.3.3 below, we start with the following extension of the interpolation in (70) to the axisymmetric case:

$$\tilde{\mathbf{E}}(\xi) = \begin{bmatrix} \xi & 0 & 0 & 0 & 0 \\ 0 & \eta & 0 & 0 & 0 \\ 0 & 0 & \xi & \eta & 0 \\ 0 & 0 & 0 & 0 & \xi\eta \end{bmatrix} \tag{75}$$

Clearly, these interpolation functions *violate* the counterpart of condition (63) since, in view of (73), we now have

$$\int_{\Gamma} \tilde{\mathbf{E}}(\xi) r(\xi) \, d\xi \neq 0 \tag{76}$$

Note that (76) no longer vanishes, owing to the presence of the factor $r(\xi)$ in the integrand. (At least) *three* alternative normalizations of our interpolation functions (75) leading to satisfaction of condition (63) are possible.

(i) Define $\mathbf{E}(\xi)$ by the relation

$$\boxed{\mathbf{E}(\xi) := \frac{r_0}{r(\xi)} \tilde{\mathbf{E}}(\xi)} \tag{77}$$

where $r_0 := r(\xi)|_{\xi = 0}$.

(ii) Alternatively, consider the following normalization:

$$\boxed{\mathbf{E}(\xi) := \tilde{\mathbf{E}}(\xi) - \frac{1}{\displaystyle\int_{\square} r(\xi) \, d\xi} \int_{\square} \tilde{\mathbf{E}}(\xi) r(\xi) \, d\xi} \tag{78}$$

A straightforward computation yields the following explicit result useful in the actual implementation of (78):

$$\mathbf{E}(\xi) = \begin{bmatrix} \xi - \bar{\xi} & 0 & 0 & 0 & 0 \\ 0 & \eta - \bar{\eta} & 0 & 0 & 0 \\ 0 & 0 & \xi - \bar{\xi} & \eta - \bar{\eta} & 0 \\ 0 & 0 & 0 & 0 & \xi\eta - \overline{\xi\eta} \end{bmatrix} \tag{79}$$

where, with the notation of Appendix I, the parameters $\bar{\xi}$, $\bar{\eta}$ and $\overline{\xi\eta}$ are given by the

expressions

$$\bar{\xi} = \frac{1}{3}\frac{\mathbf{r}^\mathrm{T}\mathbf{a}_1}{\mathbf{r}^\mathrm{T}\mathbf{a}_0}, \quad \bar{\eta} = \frac{1}{3}\frac{\mathbf{r}^\mathrm{T}\mathbf{a}_2}{\mathbf{r}^\mathrm{T}\mathbf{a}_0}, \quad \overline{\xi\eta} = \frac{1}{9}\frac{\mathbf{r}^\mathrm{T}\mathbf{h}}{\mathbf{r}^\mathrm{T}\mathbf{a}_0} \tag{80}$$

(iii) Finally, we consider the following normalization of our interpolation functions (75):

$$\mathbf{E}(\xi) = \begin{bmatrix} \xi - \bar{\xi} & 0 & 0 & 0 & 0 \\ 0 & \eta - \bar{\eta} & 0 & 0 & 0 \\ 0 & 0 & \xi - \bar{\xi} & \eta - \bar{\eta} & 0 \\ 0 & 0 & 0 & 0 & \xi\eta\dfrac{j(\xi)}{j_0 r(\xi)} \end{bmatrix} \tag{81}$$

where $\bar{\xi}$ and $\bar{\eta}$ are defined by the relations in (75). Since the Jacobian $j(\xi)$ is linear in ξ and η [see (A7)], the function in (81) associated with the hoop strain satisfies the key property

$$\int_{\scriptscriptstyle \sqcup} \left[\xi\eta\frac{j(\xi)}{j_0 r(\xi)} \right] r(\xi)\,\mathrm{d}\xi = 0 \tag{82}$$

so that the interpolation functions (61) satisfy condition (63).

The interpolation functions $\mathbf{G}(\xi)$ are obtained from either (77), (79) or (81) via the transformation (61).

Remarks 4.3.
1. The interpolation functions $\mathbf{G}(\xi)$ obtained using expression (81) coincides with an interpolation proposed by Taylor[21] based on our five-parameter interpolation (75).
2. The set of interpolation functions (81) leads to a *block diagonal* matrix $\mathbf{H}$ of the form

$$\mathbf{H} = \begin{bmatrix} \bar{\mathbf{H}}_{(4\times 4)} & \mathbf{0}_{(4\times 1)} \\ \mathbf{0}_{(1\times 4)}^\mathrm{T} & \dfrac{4}{9}\dfrac{E(1-v)}{(1+v)(1-2v)} \end{bmatrix} \tag{83}$$

Hence, the implementation of the five-parameter interpolation (81) involves essentially the same effort as the four-parameter function (70) of the plane problem. Our numerical simulations also indicate that (81) appears to be superior to the other two elements.
3. Our choice of functions (81) can be motivated with reference to a rectangular element with sides h and k. For a bilinear displacement field, the crucial mode to be considered is the following hourglass deformation:

$$u_r = \xi\eta a, \quad u_z = 0 \tag{84}$$

where $a \in \mathbb{R}$ is a constant. The strain field associated with this mode is given by

$$\varepsilon = a \begin{bmatrix} \dfrac{2\eta}{h} & 0 & \dfrac{\xi}{k} & \dfrac{\xi\eta}{r(\xi)} \end{bmatrix}^\mathrm{T} \tag{85}$$

Next, we recall the expression for the matrix of elastic moduli in the axisymmetric case:

$$\mathbf{C} = \frac{E}{(1+v)(1-2v)} \begin{bmatrix} (1-v) & v & 0 & v \\ v & (1-v) & 0 & v \\ 0 & 0 & \dfrac{1-2v}{2} & 0 \\ v & v & 0 & (1-v) \end{bmatrix} \tag{86}$$

Finally, we compute the strain energy over the element associated with the strain field obtained by adding to (84) the enhanced strain field derived from (81). A lengthy but straightforward calculation shows that the expression for the hoop strain in (81) is precisely such that the factor $(1-2v)$ disappears from the denominator and the energy remains, therefore, bounded as $v \to \frac{1}{2}$.   ■

5. MODEL PROBLEM II: MINDLIN–REISSNER PLATE BENDING THEORY

To illustrate the generality and wide range of applicability of the methodology introduced in Sections 2, 3 and 4, we consider here its application to the well-known Mindlin–Reissner plate theory.

First we summarize the variational formulation of the problem and mixed finite element interpolation following the same steps as in Section 2. Then, as an illustrative example, we consider the formulation of a new quadrilateral plate bending element with performance similar to the quadrilateral of Hughes and Tezduyar.[8]

5.1. Mixed variational formulation

Let $\mathscr{B} \subset \mathbb{R}^2$ be the domain occupied by a thick plate with thickness $h > 0$. We denote by $\omega(\mathbf{x})$ and $\Theta(\mathbf{x})$ the vertical deflection and two rotations at a point $\mathbf{x} \in \mathscr{B}$. As usual, we set

$$\mathbf{u}^{\mathrm{T}} := [\omega \quad \Theta^{\mathrm{T}}] = [\omega \quad \Theta_1 \quad \Theta_2] \tag{87}$$

The bending and transverse shear strains are

$$\boldsymbol{\kappa} = \nabla^s \Theta, \quad \boldsymbol{\varepsilon} = \nabla\omega - \Theta \tag{88}$$

respectively. A variational formulation of the (linear elastic) plate equations in which (88) is enforced via Lagrange multipliers (corresponding to transverse shear strains) is obtained via the following classical functional:

$$\Pi(\mathbf{u}, \boldsymbol{\sigma}, \boldsymbol{\varepsilon}) = \int_{\mathscr{B}} \tfrac{1}{2} \nabla^s \Theta \cdot \mathbf{C}_b \nabla^s \Theta \, \mathrm{d}V + \Pi_{\mathrm{ext}}(\mathbf{u})$$

$$+ \int_{\mathscr{B}} (\tfrac{1}{2} Ghk |\boldsymbol{\varepsilon}|^2 + \boldsymbol{\sigma} \cdot [\nabla\omega - \Theta - \boldsymbol{\varepsilon}]) \, \mathrm{d}V \tag{89}$$

where $\mathbf{C}_b$ is the matrix of bending moduli, and $\Pi_{\mathrm{ext}}(\mathbf{u})$ is the potential energy of the external loading with a standard expression. Note that for simplicity we have assumed isotropy, with G denoting the shear modulus and k the shear coefficient.

5.1.1. Modified variational formulation: Enhanced shear strain field. As in Section 2 we consider transverse shear strain fields of the form

$$\varepsilon = \underbrace{[\nabla\omega - \boldsymbol{\Theta}]}_{\text{compatible}} + \underbrace{\tilde{\varepsilon}}_{\text{enhanced}} \tag{90}$$

Substitution of (90) into (89) yields

$$\Pi(\mathbf{u}, \boldsymbol{\sigma}, \tilde{\boldsymbol{\varepsilon}}) = \Pi_s(\mathbf{u}) + \int_{\mathscr{B}} \left[\tfrac{1}{2} Ghk |\nabla\omega - \boldsymbol{\Theta} + \tilde{\boldsymbol{\varepsilon}}|^2 - \boldsymbol{\sigma} \cdot \tilde{\boldsymbol{\varepsilon}}\right] \mathrm{d}V \tag{91}$$

where $\Pi_s(\mathbf{u})$ denotes the first two terms in (89). Letting V denote the space of variations $(\eta, \boldsymbol{\Psi})$ of deflections and rotations, the condition for stationarity of the functional in (91) associated with the 'displacement' variables $\mathbf{u} = (\omega, \boldsymbol{\Theta})$ take the familiar expressions

$$\left.\begin{array}{l} \underbrace{D\Pi_s(\mathbf{u}) \cdot \boldsymbol{\Psi}}_{\substack{\text{standard bending} \\ \text{and loading} \\ \text{contributions}}} - \int_{\mathscr{B}} \boldsymbol{\Psi} \cdot Ghk \left[\nabla\omega - \boldsymbol{\Theta} + \tilde{\boldsymbol{\varepsilon}}\right] \mathrm{d}V = 0 \\[2em] \underbrace{D\Pi_s(\mathbf{u}) \cdot \eta}_{\substack{\text{standard loading} \\ \text{contributions}}} + \int_{\mathscr{B}} \nabla\eta \cdot Ghk \left[\nabla\omega - \boldsymbol{\Theta} + \tilde{\boldsymbol{\varepsilon}}\right] \mathrm{d}V = 0 \end{array}\right\} \tag{92}$$

for all variations $(\eta, \boldsymbol{\Psi}) \in V$. Equations (92) are completely standard except for the appearance of the enhanced strain field $\tilde{\varepsilon}$. As in Section 2 we shall denote by $\tilde{\mathscr{E}}$ and S the spaces of enhanced shear fields $\tilde{\gamma}$ and transverse shear forces τ, respectively. Then, associated with (91) we have the *additional stationarity conditions*

$$\left|\begin{array}{l} \int_{\mathscr{B}} \tau \cdot \tilde{\varepsilon} \, \mathrm{d}V = 0 \\[1.5em] \int_{\mathscr{B}} \tilde{\gamma} \cdot \left[-\boldsymbol{\sigma} + Ghk(\nabla\omega - \boldsymbol{\Theta}) + Ghk\tilde{\varepsilon}\right] \mathrm{d}V = 0 \end{array}\right. \tag{93}$$

for all variations $(\tau, \tilde{\gamma}) \in S \times \tilde{\mathscr{E}}$ of the transverse shear force and enhanced transverse shear strain field.

It is apparent that, aside from the change in notation and the different physical meaning of the fields $(\tau, \tilde{\gamma}) \in S \times \tilde{\mathscr{E}}$, equations (92) constitute the counterpart of $(9)_1$, *and equations* $(93)_{1,2}$ *are essentially identical to* $(9)_{2,3}$.

5.2. Mixed finite element interpolation

The interpolation subspaces $\tilde{\mathscr{E}}^h$ and S^h are again of the form (16)–(19) and are subject to the same two conditions (20) and (21). Following our developments in Section 4, we consider a concrete realization of the spaces S^h and $\tilde{\mathscr{E}}^h$ for the *four-node bi-linear isoparametric element.* We summarize the relevant definitions needed. We set

$$\tilde{\mathscr{E}}^h = \left\{\tilde{\gamma}^h = \sum_{e=1}^{n_{\text{elm}}} \tilde{\gamma}_e(\xi)\chi_e \, | \, \tilde{\gamma}_e(\xi) = \left[\frac{j_0}{j(\xi)} \mathbf{J}_0^{-\mathrm{T}} \mathbf{E}(\xi)\right]\boldsymbol{\alpha}_e \text{ with } \boldsymbol{\alpha}_e \in \mathbb{R}^{n_e}\right\} \tag{94}$$

and

$$S^h = \left\{ \tau^h = \sum_{e=1}^{n_{elm}} \tau_e(\xi) \chi_e \mid \tau_e(\xi) = \mathbf{J}_0 \mathbf{S}(\xi) \boldsymbol{\beta}_e \text{ with } \boldsymbol{\beta}_e \in \mathbb{R}^2 \times \mathbb{R}^{n_\tau} \right\} \tag{95}$$

The interpolation functions $\mathbf{S}(\xi)$ and $\mathbf{E}(\xi)$ for the stress field and enhanced strain field, respectively, are subject to the two conditions:

(i)

$$\langle \tau_e, \tilde{\gamma}_e \rangle_{L^2} = 0 \Rightarrow \int_\square \mathbf{S}^{\mathrm{T}}(\xi) \mathbf{E}(\xi) \, \mathrm{d}\xi = 0 \tag{96}$$

(ii) S^h contains piece-wise constant element transverse shear stresses; so that

$$\int_\square \mathbf{E}(\xi) \, \mathrm{d}\xi = 0 \tag{97}$$

Observe that we have employed the same notation as in Section 4.

5.2.1. The choice of isoparametric stress and enhanced strain fields. We consider the following structure of stress interpolants:

$$\mathbf{S}(\xi) = \begin{bmatrix} 1 & 0 & \eta & 0 \\ 0 & 1 & 0 & \xi \end{bmatrix} \tag{98}$$

Furthermore, we set

$$\mathbf{E}(\xi) = \begin{bmatrix} \xi & 0 & \xi\eta & 0 \\ 0 & \eta & 0 & \xi\eta \end{bmatrix} \tag{99}$$

Clearly, (98) and (99) satisfy conditions (96) and (97) above. Further, observe that $n_\varepsilon = 4 > 2$. Our numerical simulations show that the resulting element exhibits no locking response in the thin plate limit.

Remarks 5.1.
1. As noted in Section 3.2.1, the scheme can be formulated as a **B**-bar method. We note that, for Mindlin–Reissner linear isotropic plate theory, expression (37) for $\bar{\mathbf{B}}$ becomes independent of the constitutive properties since the factor Ghk cancels out. In fact,

$$\bar{\mathbf{B}} = \mathbf{B} - \mathbf{G} \left[\int_{\mathscr{B}_e} \mathbf{G}^{\mathrm{T}} \mathbf{G} \, \mathrm{d}\mathscr{B} \right]^{-1} \int_{\mathscr{B}_e} \mathbf{G}^{\mathrm{T}} \mathbf{B} \, \mathrm{d}\mathscr{B} \tag{100}$$

2. A mechanical motivation for the choice for interpolations (98) and (99) is as follows. The standard isoparametric interpolations of the displacements (ω, Θ_1 and Θ_2) are

$$\omega = a_1 + b_1 \xi + c_1 \eta + d_1 \xi\eta$$
$$\Theta_1 = a_2 + b_2 \xi + c_2 \eta + d_2 \xi\eta \tag{101}$$
$$\Theta_2 = a_3 + b_3 \xi + c_3 \eta + d_3 \xi\eta$$

Thus, for a *square element*, we have

$$\omega_{,1} = b_1 + d_1 \eta$$
$$\omega_{,2} = c_1 + d_1 \xi \tag{102}$$

Hence,

$$\omega_{,1} - \Theta_1 = (b_1 - a_2) + (d_1 - c_2)\eta - b_2\xi - d_2\xi\eta$$

$$\omega_{,2} - \Theta_2 = (c_1 - a_3) + (d_1 - b_3)\xi - c_3\eta - d_3\xi\eta$$

(103)

It follows that the enhanced transverse shear strain field $\tilde{\varepsilon}$, emanating from (99), i.e.

$$\tilde{\varepsilon}_1 = \xi\alpha_1 + \xi\eta\alpha_3$$

$$\tilde{\varepsilon}_2 = \eta\alpha_2 + \xi\eta\alpha_4$$

(104)

provides the additional terms that balance $\nabla\omega$ and Θ. Since

$$\alpha = -\left[\int_{\mathscr{B}_e} \mathbf{G}^{\mathrm{T}}\mathbf{G}\,d\mathscr{B}\right]^{-1}\int_{\mathscr{B}_e} \mathbf{G}^{\mathrm{T}}(\nabla\omega - \theta + \tilde{\varepsilon})\,d\mathscr{B}$$

(105)

a simple calculation shows (for the square element) that

$$\alpha = -\begin{Bmatrix} b_2 \\ c_3 \\ d_2 \\ d_3 \end{Bmatrix}$$

(106)

The resulting enhanced shear strain field becomes

$$\nabla\omega - \Theta + \tilde{\varepsilon} = \begin{Bmatrix} (b_1 - a_2) + (d_1 - c_2)\eta \\ (c_1 - a_3) + (d_1 - b_3)\xi \end{Bmatrix}$$

(107)

Upon expansion of the components of these expressions, the shear strain field is seen to be precisely that of the Bathe and Dvorkin[2] element; see also Bathe and Brezzi.[1]

The transformations (94) and (95) account for the case in which the element is no longer square. ∎

6. NUMERICAL SIMULATIONS

In this section we illustrate the methodology developed in the preceding sections in a number of numerical simulations. First, we show that the interpolations (69) and (70) of Section 4 exhibit comparable performance ((69) slightly superior to (70), which is equivalent to the incompatible modes element of Taylor et al.[22]). We also illustrate the excellent performance of these enhanced elements in the nearly incompressible problem by means of a well-known test problem. Next, we consider elastoplastic response and assess coarse mesh accuracy in bending dominated problems. In Section 6.3 we assess the performance of the axisymmetric elements developed in Section 4.3 and in Section 6.4 we illustrate the performance of the quadrilateral plate bending element developed in Section 5. We conclude this section with a simulation concerned with a geometrically non-linear problem.

6.1. Plane stress/plane strain elasticity

The incompatible modes element of Taylor et al.[22] has been well known to produce excellent results in bending dominated situations. It appears, however, that the excellent distortion insensitivity and coarse mesh accuracy, and the good performance of this element in the
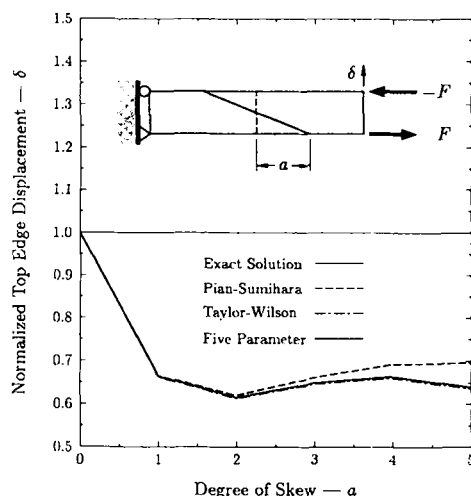
Figure 2. Beam bending problem: sensitivity to mesh distortion

incompressible limit, are not widely appreciated. We illustrate below these characteristics, and demonstrate that the performance of this element is essentially identical to recently proposed *two-field assumed stress* elements (e.g. Pian and Sumihara[11]). The five-parameter element developed in Section 4 improves upon the performance of the Taylor *et al.*[29] quadrilateral.

6.1.1. Beam bending: Sensitivity to mesh distortion. In this standard test, a beam modelled with a two-element mesh is fixed on one end and subjected to a bending moment on the other end, as shown in Figure 2. The edge separating the two elements is then gradually rotated (a distance $\pm a$ on the top and bottom surfaces) to skew the mesh. The results for this test (normalized with the exact solution) are shown in Figure 2 for the quadrilateral of Taylor *et al.*,[22] the five-parameter enhanced strain interpolation of Section 4, and the assumed stress element of Pian and Sumihara.[11] The similar distortion sensitivity performance exhibited by all these elements is noted.

6.1.2. Incompressible elasticity: Driven cavity flow. This is a standard test problem for assessing the performance of finite element formulations in the nearly incompressible limit (see e.g. Hughes[7]). The 'leaky-lid' boundary condition is employed, and the pressure results of the enhanced strain element of Section 4.2 are shown in Figures 3 for $10 \times 10, 20 \times 20$ and 40×40 element mesh configurations. The 'smoothed' stresses, obtained via an L_2 projection to the nodes, are also shown. Even though the results exhibit oscillations in the pressure, the magnitude of these oscillations is reduced with mesh refinement, and the smoothed distribution converges rapidly. This is in contrast with the well-known response exhibited by the bilinear displacement/constant pressure quadrilateral element.

Remark 6.1. We note that the pressures evaluated at the centre of the element are always in close agreement with the smoothed distribution, and hence more accurate. This observation is in complete agreement with the stress recovery procedure in Section 3.3. In effect, the stress field

over the element evaluated using the relation

$$\sigma = \mathbf{C}[\nabla^s \mathbf{u} + \bar{\boldsymbol{\varepsilon}}] \tag{108}$$

does not satisfy the orthogonality condition $(9)_2$. On the other hand, the stress field (54) obtained through the variational stress recovery is equivalent to evaluating (108) at the centre of the element. ∎
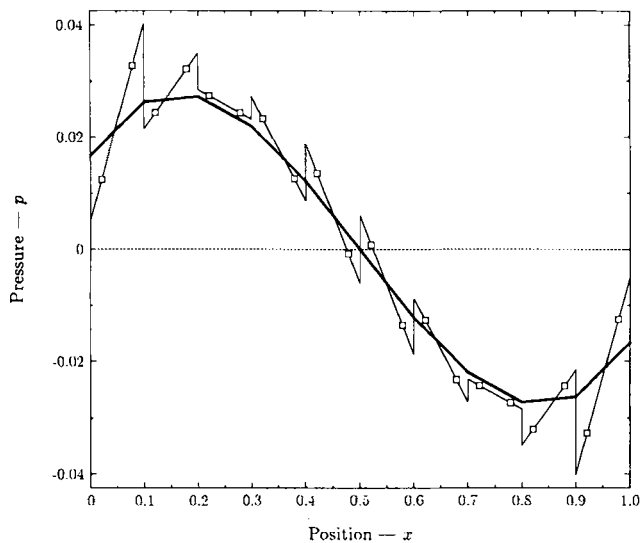

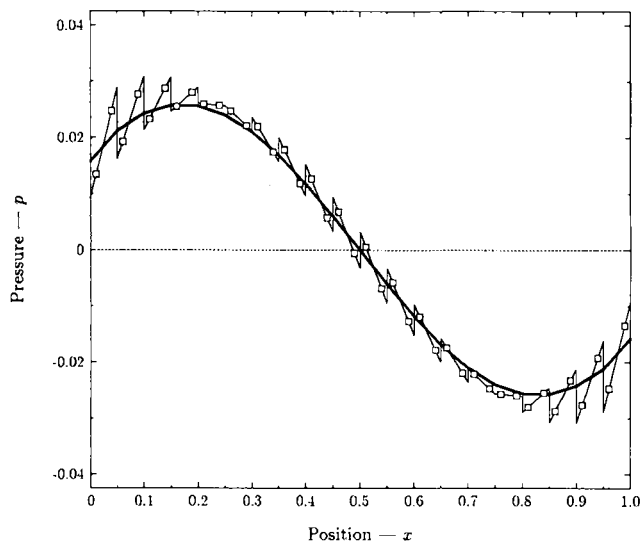Figure 3(a). Driven cavity flow problem. Pressure distribution at $y \approx 0.22$. 10×10 mesh

Figure 3(b). Driven cavity flow problem. Pressure distribution at $y \approx 0.22$. 20×20 mesh
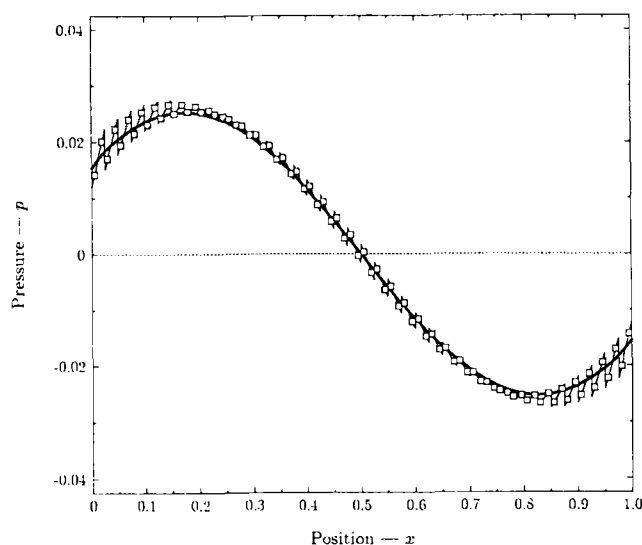
Figure 3(c). Driven cavity flow problem. Pressure distribution at $y \approx 0\cdot22$. 40×40 mesh

6.2. Plasticity and viscoplasticity: J_2-flow theory

The extension of the mixed formulation presented in Section 2 to plasticity and viscoplasticity is discussed in Appendix III. Here, we present several examples that illustrate the excellent performance of the enhanced strain elements of Section 4.3 in the elastoplastic regime. We focus our attention on the interpolation (70) which, in the linear elastic regime, is equivalent to the Taylor et al.[22] incompatible mode formulation. Several standard test problems are used to demonstrate the advantage of these enhanced elements over the standard displacement formulation, and the constant dilatation (B-bar) approach for both plane strain and plane stress problems.

6.2.1. Extension of a double edge notched specimen.
This test problem was introduced by Nagtegaal et al.[10] to demonstrate the spurious response of standard displacement models in highly constrained plane strain, axisymmetric or three dimensional elastoplastic problems. Although the problem at hand exhibits a limit load given analytically by $\sigma_{\text{lim}}^{\text{notch}} \approx 2\cdot97\sigma_Y$, where σ_Y is the flow stress, the displacement model produces a load–deflection curve which increases monotonically beyond the load limit. Perfect plasticity is assumed, and the values of the material constants are

$$E = 70, \quad v = 0\cdot3, \quad \sigma_Y = 0\cdot243 \tag{109}$$

The specimen has total width $W = 10$, height $L = 30$, and ligament thickness $b = 1$, resulting in a value of $F_{\text{lim}} \approx 0\cdot7217$ for the limit load.

The simulation is carried out by displacement controlled load steps at the top surface of the specimen. A 5×15 mesh is used to model a quarter of the problem using symmetry boundary conditions. Each displacement step corresponds to

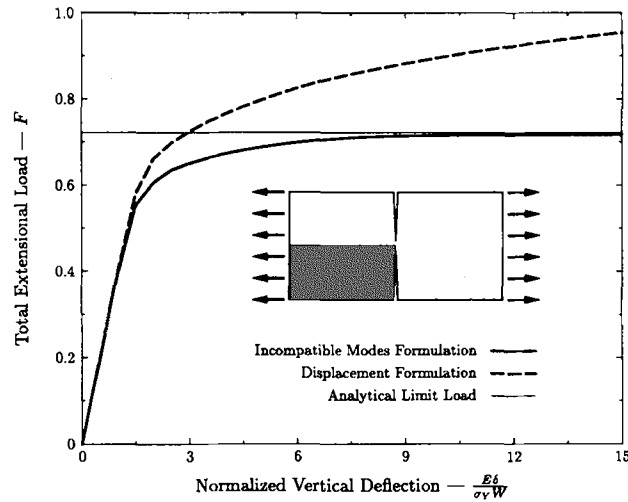$$\frac{E\Delta\delta}{\sigma_Y W} = 0\cdot5 \tag{110}$$

Figure 4. Double edge notched tension specimen: elastoplastic analysis (suggested by Nagtegaal *et al.*[10]). The load–deflection behaviour of the incompatible modes element asymptote to the analytical limit load, while the standard displacement formulation yields indefinitely increasing loads

The load–deflection plots for both the displacement and enhanced strain formulations in plane strain are shown in Figure 4 for $0 \leqslant E\delta/\sigma_Y W \leqslant 15$, where δ is the top displacement (30 time steps). Also shown is the analytical limit load. It is apparent that the displacement formulation does not exhibit any limit load, while the enhanced strain formulation element asymptotes to the analytical solution.

6.2.2. Plane strain: Cook's membrane problem. This test problem demonstrates the superior coarse mesh accuracy in bending dominated *elastoplastic* problems, and insensitivity to mesh distortion exhibited by the enhanced strain elements of Section 4 over the mean dilatation approach (**B**-bar) of Nagtegaal *et al.*[10] We consider a tapered panel, clamped on one end, and subjected to a shearing load on the other. The elastic version of this problem is known as 'Cook's membrane problem'. The simulation is performed using load control with steps of $\Delta F = 0.1$, and F ranging from 0 to 1.8. The vertical displacement of the top edge node is plotted against different mesh configurations for both formulations in Figure 5. The mean dilatation approach appears to converge to the same answer as the enhanced element; however, much finer meshes are required. In fact, the enhanced strain formulation (with interpolation given by (69)) is practically converged with an 8×8 mesh, while the mean dilatation method shows ≈ 5 per cent error, even with a 64×64 mesh (4096 elements).

J_2-flow theory with linear kinematic isotropic hardening is assumed. The values of the material constants are

$$E = 70, \quad \nu = 1/3, \quad \sigma_Y = 0.243, \quad H = 0.135, \quad K = 0.015 \qquad (111)$$

where K and H denote the isotropic and kinematic hardening modulus in uniaxial stress, respectively. This same problem was re-examined in the plane stress case, and the results compared with the assumed stress formulation based on the interpolation of Pian and Sumihara[11] using the stress driven return mapping algorithm of Simo *et al.*[18] The results
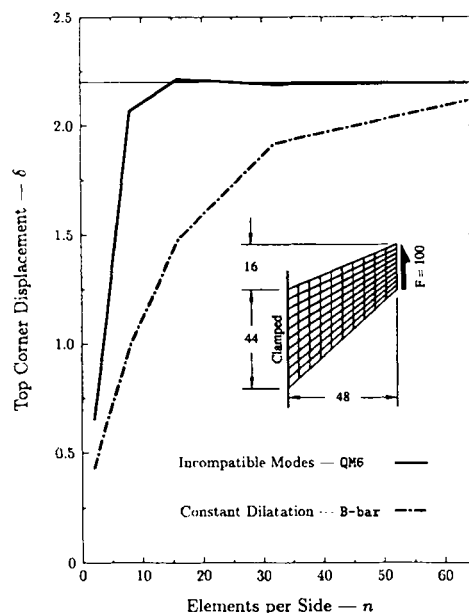
Figure 5. Cook's membrane problem: plane strain elastoplastic analysis. A clamped wing is subjected to an in-plane shearing load using several mesh configurations. The incompatible modes formulation yields practically converged results with the 8 × 8 results, while the B-bar formulation is at 5 per cent error even with a 64 × 64 mesh (4096 elements)

(shown in Figure 6) demonstrate the superior performance of both formulations over the standard displacement model. It should be noted that both the enhanced strain element and the assumed stress element exhibit essentially identical performance. However, the assumed stress element requires a non-standard (more cumbersome) return mapping algorithm, while the enhanced strain element uses the standard strain-driven return mappings.

6.2.3. Plane stress: Clamped arch problem. As a further illustration of the performance of the enhanced strain elements of Section 4 in plane stress analysis, we consider a clamped arch, of radius $R = 10$ and thickness $t = 1$, vertically loaded at the top. Again, J_2-flow theory with linear isotropic/kinematic hardening is assumed, along with the following values for the material constants:

$$E = 70, \quad v = 0.3, \quad \sigma_Y = 0.243, \quad H = 5.0, \quad K = 0.1 \tag{112}$$

Load control is employed with equal force increments of $\Delta F = 0.01$ to obtain values $0 \leqslant F \leqslant 0.2$ of the applied force. The vertical top displacement is plotted against the number of elements in the radial direction for both formulations in Figure 7. The superior performance exhibited by the enhanced element (with interpolation (70)) over the standard displacement formulation is apparent from these results.

6.2.4. Viscoplasticity. As a final illustration, we consider viscoplastic response. A perforated strip is modelled using a 72 element mesh on a quarter of the specimen using symmetry boundary conditions, and displacement control in steps of $\Delta \delta = 0.03$, for the range $0 \leqslant \delta \leqslant 0.45$. We
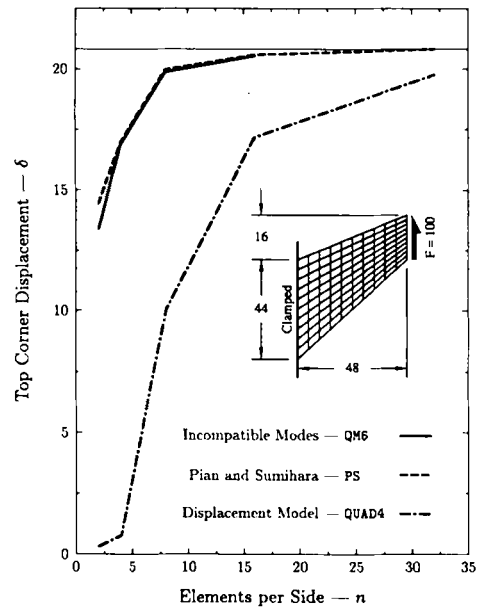
Figure 6. Cook's membrane problem: plane stress elastoplastic analysis. The incompatible modes formulation yields almost identical results to the (more cumbersome) assumed stress method of Simo *et al.*[18] The pure displacement formulation exhibits much slower convergence with mesh refinement
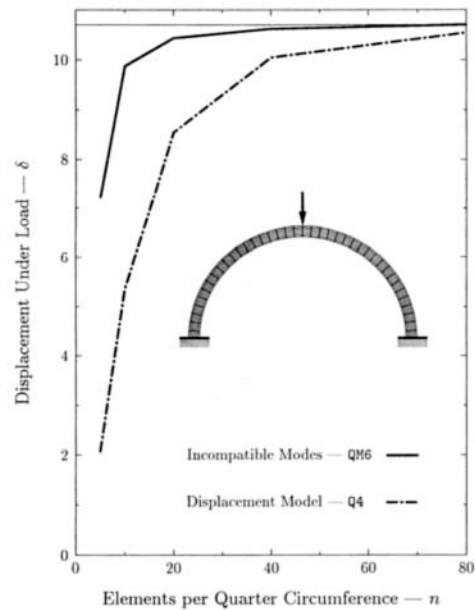

Figure 7. Clamped arch problem: plane stress elastoplastic analysis. The advantage of the incompatible modes formulation over the pure displacement model is again manifest, even for problems with no incompressibility locking

assume linear isotropic/kinematic J_2-viscoplasticity of the Duvaut–Lions type, as described in Simo *et al.*[17] The material properties are

$$E = 70, \quad v = 0.3, \quad \sigma_Y = 0.243, \quad H = 0.135, \quad K = 0.015 \qquad (113)$$

The load–deflection curves for this problem using both plane stress and plane strain analysis are plotted in Figures 8 and 9, respectively for the following values of the viscosity coefficient: $\eta = 0$ (inviscid case) $\eta = 1$, $\eta = 5$, $\eta = 25$.
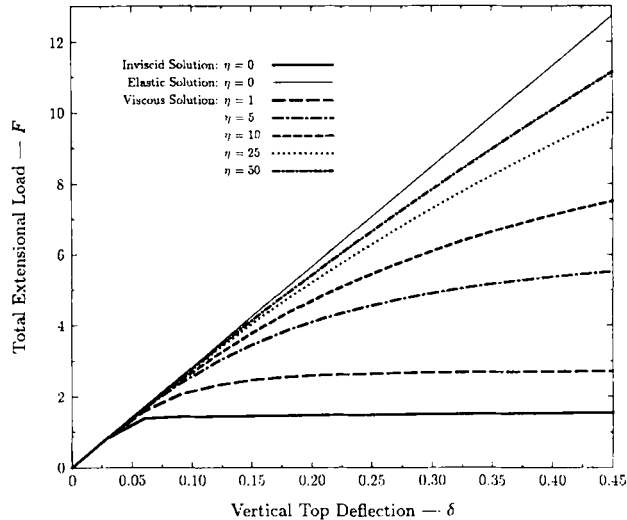

Figure 8. Viscoplastic analysis of the perforated strip problem. Plane strain case. A 72 element mesh is used on a quadrant of the problem, and the load–deflection plots are shown for different values of viscosity
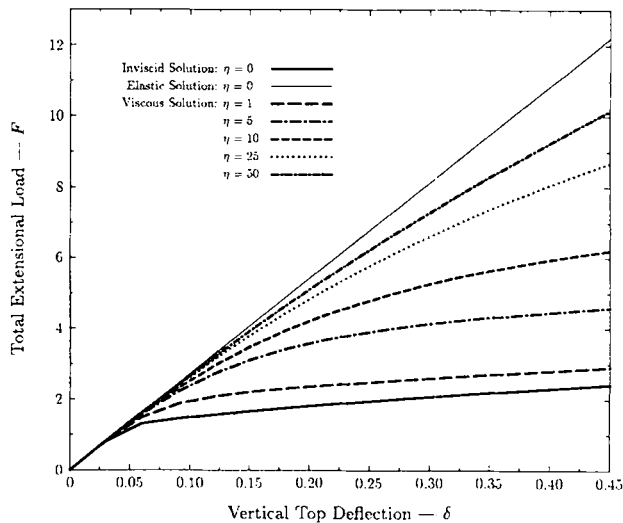

Figure 9. Viscoplastic analysis of the perforated strip problem. Plane stress case. A 72 element mesh is used on a quadrant of the problem, and the load–deflection plots are shown for different values of viscosity

6.3. Axisymmetric elasticity elements

The performance of the axisymmetric elements developed in Section 4.3 is demonstrated in three representative examples. The element defined by the interpolations (77) will be referred to as element 'A', the element defined by the interpolations (79) will be referred to as element 'B' and the element defined by the interpolations (81) will be referred to as element 'C'. The effect of the Poisson's ratio on the performance of these proposed elements is shown to be minimal, and no 'locking' is observed in the nearly incompressible limit.

6.3.1. *Expansion of a thick cylinder.* A thick walled cylinder of inner radius $R_i = 3$ and outer radius $R_o = 9$ is subjected to an internal pressure $p = 1$. The thickness of the cylinder is $t = 1$, and plane strain conditions are assumed in the z-direction. The modulus of elasticity is $E = 1000$ and the Poisson's ratio is varied between 0·0 and 0·4999 to examine the effects of incompressibility. The exact solution to this problem is given by

$$u = \frac{(1 + v)pR_i^2}{E(R_o^2 - R_i^2)}[R_o^2/r + (1 - 2v)r] \tag{114}$$

The displacement at $r = R_i$ is then given by

$$u|_{r=3} = \frac{(1 + v)}{8}[27 + 3(1 - 2v)] \times 10^{-3} \tag{115}$$

A five-element mesh is used in two configurations: one regular and the other skewed, as shown in Figure 10. The results are listed in Table I for the regular mesh and in Table II for the skewed mesh. All elements yield almost exact results for this problem, and no degradation occurs in the incompressible limit for either mesh.
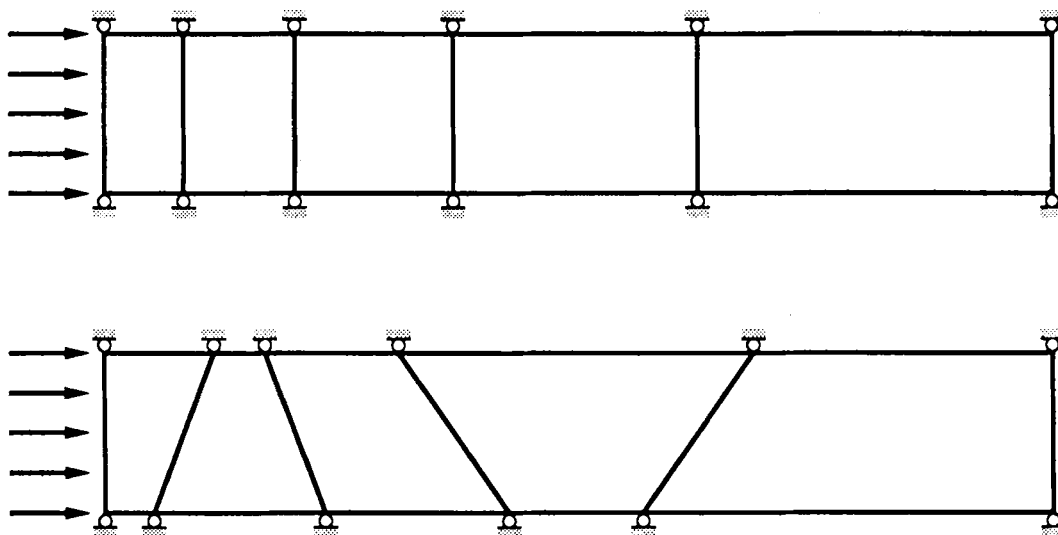

Figure 10. The extension of the thick cylinder expansion problem is modelled with one row of 5 axisymmetric elements in the radial direction, using a regular and skewed mesh

Table I. Thick walled cylinder. Regular mesh

	Displacement $\times 10^{-3}$			
v	Element A	Element B	Element C	Exact
0·0	3·72611	3·72611	3·72611	3·7500
0·25	4·41340	4·41340	4·41340	4·4531
0·3	4·53826	4·53826	4·53826	4·5825
0·49	4·97054	4·97055	4·97055	5·0399
0·499	4·98921	4·98921	4·98921	5·0602
0·4999	4·99107	4·99107	4·99107	5·0623

Table II. Thick walled cylinder. Skewed mesh

	Displacement $\times 10^{-3}$			
v	Element A	Element B	Element C	Exact
0·0	3·72361	3·72355	3·72666	3·7500
0·25	4·41005	4·40991	4·41540	4·4531
0·3	4·53463	4·53447	4·54076	4·5825
0·49	4·96376	4·96375	4·97625	5·0399
0·499	4·98207	4·98209	4·99514	5·0602
0·4999	4·98388	4·98391	4·99702	5·0623

6.3.2. Bending of a thin cylinder. A cylindrical shell of median radius $R = 167·5$, length $L = 51$, thickness $h = 1$ and Young's modulus $E = 11\,250$ is subjected to an end moment $M = 2000$, as shown in Figure 11. The exact (shell) solution for the deflection under the moment is given by

$$w_{\max} = \frac{M}{2\beta^2 D}, \quad \beta^4 = \frac{Eh}{4R^2 D}, \quad D = \frac{Eh^3}{12(1 - v^2)} \tag{116}$$

The cylinder is modelled with one row of 17 elements (aspect ratio 3) and the results are shown in Table III for different values of the Poisson's ratio. Again, the three elements yield almost exact results for this problem, and no degradation occurs in the incompressible limit.

6.3.3. Bending of a circular plate. A circular plate of radius $R = 10$, thickness $h = 1$ and Young's modulus $E = 1875$ is subjected to a uniform loading $q = 1$, as shown in Figure 12. The
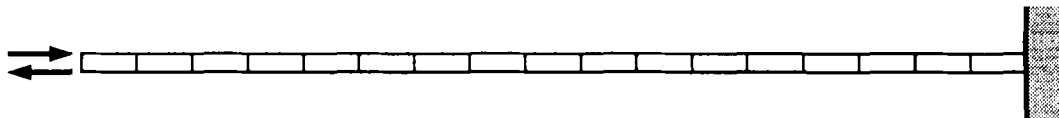

Figure 11. The bending of a thin cylinder problem is modelled using one row of 17 axisymmetric elements in the axial direction. The radius is 167·5 and the thickness is 1

Table III. Bending of a thin cylinder

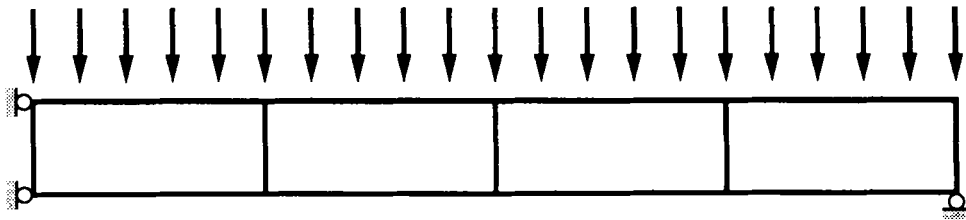|	Displacement under the moment			
v	Element A	Element B	Element C	Exact
0·0	0·60637	0·60637	0·60637	0·6158
0·25	0·58708	0·58708	0·58708	0·5963
0·3	0·57845	0·57845	0·57845	0·5875
0·49	0·52889	0·52899	0·52899	0·5368
0·499	0·52580	0·52580	0·52580	0·5337
0·4999	0·52548	0·52549	0·52548	0·5334

Figure 12. The circular plate bending problem is modelled using one row of 4 axisymmetric elements in the radial direction. The thickness is 1, and the plate is subjected to a uniform load $q = 1$ in the z-direction

exact (plate) solution for the central displacement is given by

$$w_{\text{max}} = \frac{qR^4}{64D}\left(\frac{5+v}{1+v} + \frac{4}{3}\frac{3+v}{1-v^2}\frac{h^2}{R^2}\right), \quad D = \frac{Eh^3}{12(1-v^2)} \tag{117}$$

The results for this problem (listed in Table IV) exhibit some dependence for elements A and B on the values of the Poisson's ratio used. However, the performance of element C is practically

Table IV. Bending of a circular plate

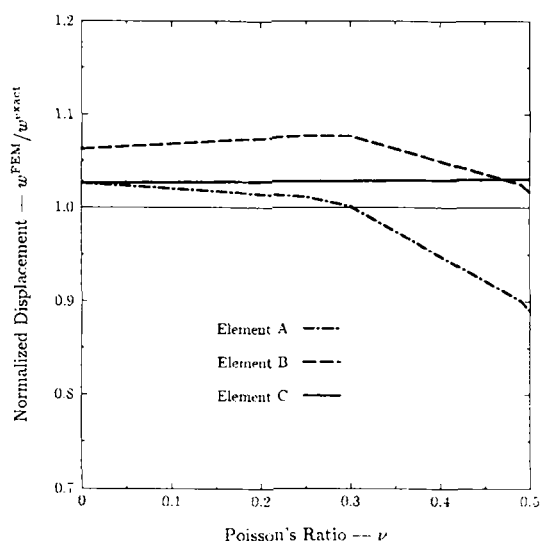|	Central displacement			
v	Element A	Element B	Element C	Exact
0·0	5·16485	5·34791	5·16485	5·0320
0·25	4·01647	4·27654	4·08232	3·9707
0·3	3·74893	4·03096	3·85023	3·7436
0·49	2·55261	2·90557	2·92096	2·8248
0·499	2·48632	2·83936	2·87508	2·7900
0·4999	2·47963	2·83264	2·87048	2·7855

Figure 13. The effect of the Poisson's ratio on the performance of the axisymmetric elements. Elements A and B show deterioration of performance with increasing incompressibility, while element C maintains excellent performance over the whole range of v

insensitive to the value of the Poisson ratio. For element A (interpolation (77)), the element is 2 per cent soft for $v = 0$ and 11 per cent stiff for $v = 0.4999$; for element B (interpolation (79)), the element is 6 per cent soft for $v = 0$ and 1 per cent soft for $v = 0.4999$, whereas for element C (interpolation (81)), the element is 2.5 per cent soft for $v = 0$ an 3 per cent soft for $v = 0.4999$. This dependence of elements A and B on the Poisson's ratio is illustrated in Figure 13.

6.4. Plate bending element

In this section we illustrate the performance of the Mindlin–Reissner plate bending element developed in Section 5. Three different eometries are used: a square plate, a rhombic plate and a circular plate. The results are compared to the quadrilateral element of Hughes and Tezduyar[8] (referred to as T1 in what follows). As noted in Remarks 4.1, the present element is identical for a square mesh to the T1 element, and hence the results are the same for the square plate problem. The rhombic plate configuration results in a mesh of rhombic shaped elements, and the present element seems to perform slightly better than T1 in this configuration. However, for the circular plate problem, the T1 element performs better. Nevertheless, the element of Section 5 is a 'decent performer' which illustrates the use of enhanced strain interpolations in the construction of locking-free plate bending elements.

6.4.1. Bending of a square plate. A simply supported square plate of side length $L = 10$, thickness $h = 0.1$, modulus of elasticity $E = 10.92$ and Poisson's ratio of $v = 0.3$ is subjected to a uniform load $q = 1$. This problem is modelled using symmetry boundary conditions on a quadrant. Since the mesh is square, the results of our element and the T1 element (Table V) are identical, consistent with Remarks 4.1.

Table V. Bending of a square plate

Mesh	Central displacement $\times 10^4$		
	Present	T1	Series
2×2	3·9712	3·9712	4·0644
4×4	4·0436	4·0436	4·0644
8×8	4·0593	4·0593	4·0644
16×16	4·0632	4·0632	4·0644

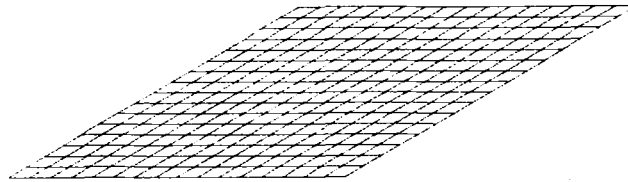Figure 14. Rhombic plate mesh

6.4.2. Bending of a rhombic plate. A simply supported $30°$ skew plate of side length $L = 100$, thickness $t = 1$, modulus of elasticity $E = 10^3$ and Poisson's ratio $v = 0·3$ is subjected to a uniform loading $q = 1$. The exact solution to this problem includes singularities in the moments at the obtuse vertices. and the problem has been considered by some to be a non-representative numerical test. The mesh configuration shown in Figure 14 is used to model the full plate, resulting in rhombic shaped elements. The results listed in Table VI indicate that the present 'enhanced strain' element performs slightly superior to the T1 element in this problem.

6.4.3. Bending of a circular plate. A simply supported circular plate of radius $R = 5$, thickness $t = 0·1$, modulus of elasticity $E = 10·92$ and Poisson's ratio $v = 0·3$ is subjected to a uniform load $q = 1$. A quadrant of the problem is modelled using symmetry boundary conditions, using the mesh configuration shown in Figure 15. This mesh configuration imposes severe distortion on the elements, and as shown in Table VII, the T1 element is superior to the present element. Nevertheless, the present element is locking-free and exhibits reasonable behaviour eve   in this case.

6.5. Geometrically non-linear problem: Compressible neo-Hookean material

The extension of the method described in Section 2 to the geometrically non-linear regime will be addressed in a subsequent publication. Here, we shall merely illustrate the performance of this

Table VI. Bending of a rhombic plate

Central displacement × 10^{-2}			
Mesh	Present	T1	Series
4 × 4	3·93046	3·9159	4·455
8 × 8	3·98412	3·8803	4·455
16 × 16	4·27274	4·1565	4·455
32 × 32	4·46680	4·3882	4·455

Table VII. Bending of a circular plate

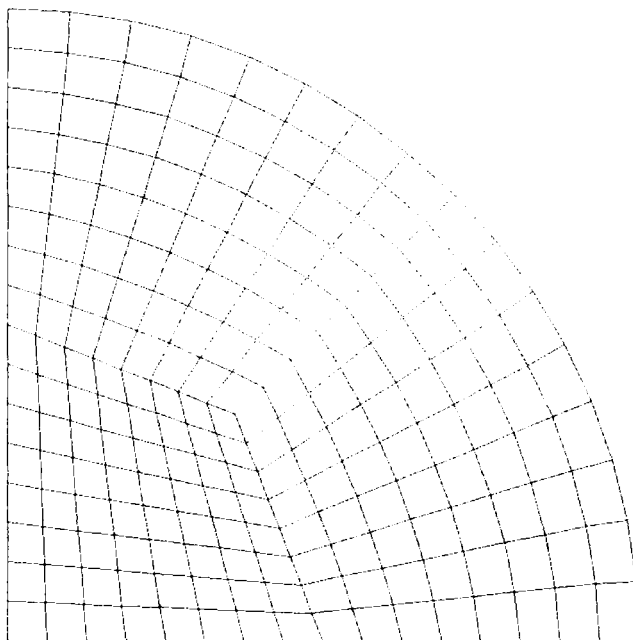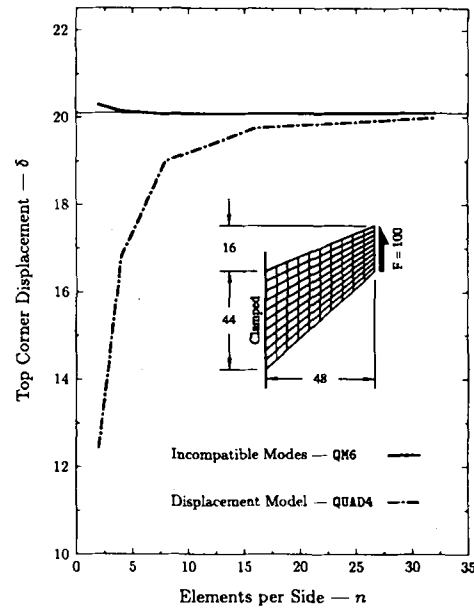| Central displacement × 10^4			
Mesh	Present	T1	Series
12 elmts	3·6966	3·9070	3·9831
48 elmts	3·9140	3·9649	3·9831
192 elmts	3·9664	3·9789	3·9831
768 elmts	3·9791	3·9822	3·9831

Figure 15. Circular plate mesh

Figure 16. Cook's membrane problem: compressible neo-Hookean material model

formulation in the context of the non-linear version of the element described in Section 4.2. We consider once more Cook's membrane problem, described in Section 6.2.2, but now in the non-linear regime for an elastic material characterized by the following stored energy function:

$$W := \lambda \frac{(J^2 - 1)}{4} - \left(\frac{\lambda}{2} + \mu\right) \ln J + \frac{1}{2}\mu(\text{tr } C - 3) \tag{118}$$

where C is the Cauchy–Green strain tensor, and J is the Jacobian determinant of the deformation gradient. The dimensions of the problem remain the same as in Section 6.2.2, and the new material properties are $\lambda = 52\cdot5$ and $\mu = 26\cdot25$. In Figure 16, we compare the results obtained with the standard bilinear element with constant volume and constant pressure, as described in Simo et al.,[19] and the non-linear version of the quadrilateral element in Section 4.2. The advantage of the latter formulation over the former is manifest.

7. CONCLUDING REMARKS

We have presented a class of assumed mixed finite element methods which allows the systematic development of low order elements possessing good coarse mesh and distortion insensitivity

properties. We have shown that well-known incompatible mode element formulations arise in the present context merely as particular (*conforming*) interpolations of the enhanced strain field. We have illustrated the methodology with the development of new plane, axisymmetric and plate bending elements. Furthermore, we have shown that assumed stress low order quadrilaterals, currently perceived as possessing nearly optimal accuracy and distortion insensitivity in coarse meshes, exhibit essentially the same performance as the assumed strain enhanced elements considered in this paper.

Constitutive equations in non-linear solid mechanics typically define a stress tensor in terms of a suitable conjugate strain measure. Assumed strain methods use these *direct constitutive relations* in a three-field variational setting. Assumed stress methods, on the other hand, employ *inverse constitutive relations* which define strains in terms of stress measures in the context of a two-field variational formulation. Well-known and widely used constitutive models, such as finite deformation elasticity, demonstrate that explicit expressions for these inverse relations are generally not available. Furthermore, at the constitutive level, the standard algorithmic framework in non-linear solid mechanics is typically *strain driven*; this is the case for the standard return mapping algorithms of plasticity. For these reasons, from a practical standpoint, we believe that *assumed strain* mixed methods are much better suited than *assumed stress* methods for non-linear analysis.

APPENDIX I. ANALYSIS OF WILSON'S QUAD

In this Appendix, we summarize some results needed on isoparametric elements, we derive an explicit expression for the interpolation matrix $G(\xi)$ of the original incompatible mode of Wilson *et al.*,[25] and we give an explicit characterization of the constant stress states that violate the patch test.

We write the bilinear isoparametric interpolations as

$$\left.\begin{array}{l} x = \mathbf{x}^\mathrm{T}\mathbf{N}(\boldsymbol{\xi}), \quad y = \mathbf{y}^\mathrm{T}\mathbf{N}(\boldsymbol{\xi}) \\ \mathbf{N}(\boldsymbol{\xi}) := \mathbf{a}_0 + \mathbf{a}_1\xi + \mathbf{a}_2\eta + \mathbf{h}\xi\eta \end{array}\right\} \tag{A1}$$

where $\boldsymbol{\xi} = (\xi, \eta)$ and

$$\begin{aligned} \mathbf{a}_0 &= \tfrac{1}{4}[1 \quad 1 \quad 1 \quad 1]^\mathrm{T} \\ \mathbf{a}_1 &= \tfrac{1}{4}[-1 \quad 1 \quad 1 \quad 1]^\mathrm{T} \\ \mathbf{a}_2 &= \tfrac{1}{4}[-1 \quad -1 \quad 1 \quad 1]^\mathrm{T} \\ \mathbf{h} &= \tfrac{1}{4}[1 \quad -1 \quad 1 \quad -1]^\mathrm{T} \\ \mathbf{x} &= [x_1 \quad x_2 \quad x_3 \quad x_4]^\mathrm{T} \\ \mathbf{y} &= [y_1 \quad y_2 \quad y_3 \quad y_4]^\mathrm{T} \end{aligned} \tag{A2}$$

Here, $\mathbf{x}_A = (x_A, y_A)$, $A = 1, \ldots, 4$, are the co-ordinates of the nodal points of a typical element $\mathscr{B}_e$. The Jacobian of the isoparametric map can then be written as

$$\mathbf{J}(\boldsymbol{\xi}) = \begin{bmatrix} \dfrac{\partial x}{\partial \xi} & \dfrac{\partial x}{\partial \eta} \\ \dfrac{\partial y}{\partial \xi} & \dfrac{\partial y}{\partial \eta} \end{bmatrix} = \begin{bmatrix} \mathbf{x}^\mathrm{T}\mathbf{N}_{,\xi} & \mathbf{x}^\mathrm{T}\mathbf{N}_{,\eta} \\ \mathbf{y}^\mathrm{T}\mathbf{N}_{,\xi} & \mathbf{y}^\mathrm{T}\mathbf{N}_{,\eta} \end{bmatrix} \tag{A3}$$

with

$$\mathbf{N}_{,\xi} = \mathbf{a}_1 + \eta\mathbf{h}, \quad \mathbf{N}_{,\eta} = \mathbf{a}_2 + \xi\mathbf{h} \tag{A4}$$

Next, following Wilson et al.,[25] consider the following incompatible displacement interpolation:

$$\tilde{\mathbf{u}}(\xi) = \tfrac{1}{2}\underbrace{(1 - \xi^2)}_{\tilde{N}^1(\xi)}\boldsymbol{\alpha}_1 + \tfrac{1}{2}\underbrace{(1 - \eta^2)}_{\tilde{N}^2(\eta)}\boldsymbol{\alpha}_2 \tag{A5}$$

The derivatives of the incompatible shape functions $\tilde{N}^A$ relative to the Cartesian co-ordinates are obtained via standard transformation with $F^{-\mathrm{T}}$ as

$$\begin{Bmatrix} \tilde{N}^A_{,x} \\ \tilde{N}^A_{,y} \end{Bmatrix} = \frac{1}{j(\xi)} \left\{ \begin{bmatrix} \mathbf{y}^\mathrm{T}\mathbf{a}_2 & -\mathbf{y}^\mathrm{T}\mathbf{a}_1 \\ -\mathbf{x}^\mathrm{T}\mathbf{a}_2 & \mathbf{x}^\mathrm{T}\mathbf{a}_1 \end{bmatrix} + \begin{bmatrix} \xi\mathbf{y}^\mathrm{T}\mathbf{h} & -\eta\mathbf{y}^\mathrm{T}\mathbf{h} \\ -\xi\mathbf{x}^\mathrm{T}\mathbf{h} & \eta\mathbf{x}^\mathrm{T}\mathbf{h} \end{bmatrix} \right\} \begin{Bmatrix} \tilde{N}^A_{,\xi} \\ \tilde{N}^A_{,\eta} \end{Bmatrix} \tag{A6}$$

where

$$j(\xi) := \det[\mathbf{J}(\xi)] = j_0 + j_1\xi + j_2\eta \tag{A7}$$

The constants j_0, j_1 and j_2 can be easily computed in terms of $\mathbf{a}_0, \mathbf{a}_1, \mathbf{a}_2, \mathbf{h}$ and $(\mathbf{x}, \mathbf{y})$ using (A3) and (A7).

We then consider an enhanced strain field that is derived from the incompatible displacement field as

$$\tilde{\varepsilon}_{ij} = \tfrac{1}{2}(\tilde{u}_{i,j} + \tilde{u}_{j,i}) \tag{A8}$$

where a comma indicates differentiation with respect to Cartesian co-ordinates. From (A5), (A6) and (A8), we thus obtain

$$\tilde{\boldsymbol{\varepsilon}} = \mathbf{G}^1\boldsymbol{\alpha}_1 + \mathbf{G}^2\boldsymbol{\alpha}_2 = \mathbf{G}\begin{Bmatrix} \boldsymbol{\alpha}_1 \\ \boldsymbol{\alpha}_2 \end{Bmatrix} \tag{A9}$$

with

$$\mathbf{G} = \frac{1}{j(\xi)}\begin{bmatrix} -\mathbf{y}^\mathrm{T}\mathbf{a}_2\xi & 0 & \mathbf{y}^\mathrm{T}\mathbf{a}_1\eta & 0 \\ 0 & \mathbf{x}^\mathrm{T}\mathbf{a}_2\xi & 0 & -\mathbf{x}^\mathrm{T}\mathbf{a}_1\eta \\ \mathbf{x}^\mathrm{T}\mathbf{a}_2\xi & -\mathbf{y}^\mathrm{T}\mathbf{a}_2\xi & -\mathbf{x}^\mathrm{T}\mathbf{a}_1\eta & \mathbf{y}^\mathrm{T}\mathbf{a}_1\eta \end{bmatrix}$$

$$+ \frac{1}{j(\xi)}\begin{bmatrix} -\mathbf{y}^\mathrm{T}\mathbf{h}\xi^2 & 0 & \mathbf{y}^\mathrm{T}\mathbf{h}\eta^2 & 0 \\ 0 & \mathbf{x}^\mathrm{T}\mathbf{h}\xi^2 & 0 & -\mathbf{x}^\mathrm{T}\mathbf{h}\eta^2 \\ \mathbf{x}^\mathrm{T}\mathbf{h}\xi^2 & -\mathbf{y}^\mathrm{T}\mathbf{h}\xi^2 & -\mathbf{x}^\mathrm{T}\mathbf{h}\eta^2 & \mathbf{y}^\mathrm{T}\mathbf{h}\eta^2 \end{bmatrix} \tag{A10}$$

Observe from this expression that

$$\bar{\mathbf{G}} := \int_\square \mathbf{G}(\xi)j(\xi)\,\mathrm{d}\xi = \frac{4}{3}\begin{bmatrix} -\mathbf{y}^\mathrm{T}\mathbf{h} & 0 & \mathbf{y}^\mathrm{T}\mathbf{h} & 0 \\ 0 & \mathbf{x}^\mathrm{T}\mathbf{h} & 0 & -\mathbf{x}^\mathrm{T}\mathbf{h} \\ \mathbf{x}^\mathrm{T}\mathbf{h} & -\mathbf{y}^\mathrm{T}\mathbf{h} & -\mathbf{x}^\mathrm{T}\mathbf{h} & \mathbf{y}^\mathrm{T}\mathbf{h} \end{bmatrix} \neq \mathbf{0} \tag{A11}$$

Hence, *condition (30) is generally violated unless* $\mathbf{x}^\mathrm{T}\mathbf{h} = \mathbf{y}^\mathrm{T}\mathbf{h} = 0$; i.e. for a square (or parallelogram) element. Recall that the classical convergence proof for Wilson's element depends crucially on the assumption of square geometry; see Ciarlet (Reference 5, p. 260).
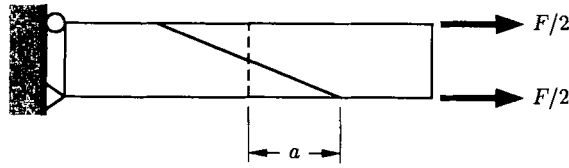
Figure 17. Example of a patch test on a 'distorted' mesh satisfied by the Wilson *et al.*[25] incompatible modes element

1. The kernel of $\bar{G}^T$

It is of interest to compute explicitly, the constant stress states for which condition (30) is violated. From expression (A11), we easily compute that

$$\tau_1 := \left\{ \begin{array}{c} y^T h \\ 0 \\ -x^T h \end{array} \right\} \quad \text{and} \quad \tau_2 := \left\{ \begin{array}{c} 0 \\ x^T h \\ -y^T h \end{array} \right\} \tag{A12}$$

are such that

$$\bar{G}^T \tau_\alpha \neq 0, \quad \alpha = 1, 2 \tag{13}$$

On the other hand, the vector τ_3 orthogonal to τ_1 and τ_2, and thus given by

$$\tau_3 = \left\{ \begin{array}{c} (x^T h)^2 \\ (y^T h)^2 \\ (x^T h)(y^T h) \end{array} \right\} \tag{A14}$$

is such that

$$\bar{G}^T \tau_3 = 0 \Rightarrow \ker[\bar{G}^T] = \text{span}\{\tau_3\} \tag{A15}$$

This result explains why the Wilson element passes patch tests on certain distorted meshes, such as the one shown in Figure 17.

For the example in Figure 17, we have $y^T h = 0$ in both elements. Thus, (A14) gives $\tau_3^T = [1 \quad 0 \quad 0]$. Since the kernel of $\bar{G}^T$ contains the solution $\sigma = [\sigma \quad 0 \quad 0]$, the element passes this patch test.

APPENDIX II. ENHANCED STRAIN INTERPOLATION

In this Appendix, we give an explicit expression for the interpolation matrix $E(\xi)$ in isoparametric space, associated with the original incompatible mode element of Wilson *et al.*[25]

Recall that the 'incompatible' displacement field is

$$\tilde{u} = \tilde{N}^1(\xi)\bar{\alpha}_1 + \tilde{N}^2(\eta)\bar{\alpha}_2 \tag{A16}$$

where $\tilde{N}^A$ are the incompatible shape functions:

$$\tilde{N}^1(\xi) = \tfrac{1}{2}(1 - \xi^2), \quad \tilde{N}^2(\eta) = \tfrac{1}{2}(1 - \eta^2) \tag{A17}$$

The covariant basis vectors associated with the isoparametric map are

$$\mathbf{g}_\xi = \left\{ \begin{array}{c} \mathbf{x}^T \mathbf{a}_1 \\ \mathbf{y}^T \mathbf{a}_1 \end{array} \right\} + \eta \left\{ \begin{array}{c} \mathbf{x}^T \mathbf{h} \\ \mathbf{y}^T \mathbf{h} \end{array} \right\} \qquad \mathbf{g}_\eta = \left\{ \begin{array}{c} \mathbf{x}^T \mathbf{a}_2 \\ \mathbf{y}^T \mathbf{a}_2 \end{array} \right\} + \xi \left\{ \begin{array}{c} \mathbf{x}^T \mathbf{h} \\ \mathbf{y}^T \mathbf{h} \end{array} \right\}$$
$$= \mathbf{g}_1^0 + \eta \mathbf{g}, \qquad\qquad = \mathbf{g}_2^0 + \xi \mathbf{g} \tag{A18}$$

where $\mathbf{x}, \mathbf{y}, \mathbf{a}_1, \mathbf{a}_2$ and $\mathbf{h}$ are as in Appendix I. The strain field in isoparametric space is then given by

$$\tilde{E} = \left\{ \begin{array}{c} \tilde{\mathbf{u}}_{,\xi} \cdot \mathbf{g}_\xi \\ \tilde{\mathbf{u}}_{,\eta} \cdot \mathbf{g}_\eta \\ \tilde{\mathbf{u}}_{,\eta} \cdot \mathbf{g}_\xi + \tilde{\mathbf{u}}_{,\xi} \cdot \mathbf{g}_\eta \end{array} \right\} \tag{A19}$$

From (A16)–(A19), we conclude that

$$\tilde{E} = \begin{bmatrix} \xi & 0 & 0 & 0 & \xi\eta & 0 \\ 0 & \eta & 0 & 0 & 0 & \xi\eta \\ 0 & 0 & \xi & \eta & \xi^2 & \eta^2 \end{bmatrix} \left\{ \begin{array}{c} -\boldsymbol{\alpha}_1 \cdot \mathbf{g}_1^0 \\ -\boldsymbol{\alpha}_2 \cdot \mathbf{g}_2^0 \\ -\boldsymbol{\alpha}_1 \cdot \mathbf{g}_2^0 \\ -\boldsymbol{\alpha}_2 \cdot \mathbf{g}_1^0 \\ -\boldsymbol{\alpha}_1 \cdot \mathbf{g} \\ -\boldsymbol{\alpha}_2 \cdot \mathbf{g} \end{array} \right\} \tag{A20}$$

Since $\mathbf{g}_1^0$, $\mathbf{g}_2^0$ and $\mathbf{g}$ are generally independent, it follows that (A20) defines the six-parameter interpolation (65).

APPENDIX III. EXTENSION TO PLASTICITY

We present in this Appendix the extension of the formulation and solutions algorithms developed in Section 2 to include inelastic effects; in particular, plasticity and viscoplasticity. We emphasize that all the standard *strain driven return mapping algorithms for plasticity and viscoplasticity carry over without any modification* to the present mixed finite element context.

1. Local strain driven return mapping algorithm

Let $\phi(\boldsymbol{\sigma}, \mathbf{q}) \leqslant 0$ denote the yield condition in stress space, let $\mathbf{q}$ be the set of generalized hardening variables and let $\boldsymbol{\varepsilon}^p$ denote the plastic strain. Without loss of generality we assume that the tensor of elastic moduli $\mathbf{C} = $ constant, and that the matrix of generalized hardening moduli, denoted by $\mathbf{D}$, is also constant. The integration of the classical equations of associative plasticity is based on the following return mapping algorithm (see Simo and Hughes[14] for a detailed account and further references to the subject).

Step 1. For a given initial data $\{\boldsymbol{\varepsilon}_n^p, \mathbf{q}_n\}$ and *given total strain* $\boldsymbol{\varepsilon}_{n+1}$, compute the trial elastic state

$$\left. \begin{array}{l} \boldsymbol{\sigma}_{n+1}^{\text{trial}} := \mathbf{C} \left[\boldsymbol{\varepsilon}_{n+1} - \boldsymbol{\varepsilon}_n^p \right] \\ \phi_{n+1}^{\text{trial}} := \phi(\boldsymbol{\sigma}_{n+1}^{\text{trial}}, \mathbf{q}_n) \end{array} \right\} \tag{A21}$$

Step 2. If $\phi_{n+1}^{\text{trial}} < 0$, the final state is the trial state $(\sigma_{n+1}^{\text{trial}}, \mathbf{q}_n)$. If, on the other hand, $\phi_{n+1}^{\text{trial}} > 0$, find $(\sigma_{n+1}, \mathbf{q}_{n-1})$ by solving the constrained optimization problem

$$
\left.
\begin{aligned}
\sigma_{n+1} &= \sigma_{n+1}^{\text{trial}} - \Delta\gamma\mathbf{C}\frac{\partial\phi}{\partial\sigma}(\sigma_{n+1}, \mathbf{q}_{n+1}) \\[4pt]
\varepsilon_{n+1}^{\text{p}} &= \varepsilon_n^{\text{p}} + \Delta\gamma\frac{\partial\phi}{\partial\sigma}(\sigma_{n+1}, \mathbf{q}_{n+1}) \\[4pt]
\mathbf{q}_{n+1} &= \mathbf{q}_n - \Delta\gamma\mathbf{D}\frac{\partial\phi}{\partial\mathbf{q}}(\sigma_{n+1}, \mathbf{q}_{n+1}) \\[4pt]
\phi(\sigma_{n+1}, \mathbf{q}_{n+1}) &= 0
\end{aligned}
\right\}
\tag{A22}
$$

For plane strain and 3-D J_2-flow theory, the preceding algorithm reduces to the well-known radial return method of Wilkins[24] and Krieg and Key.[9] For plane stress J_2-flow theory algorithm (A22) reduces to the return map of Simo and Taylor.[15]

The essential point to be noted is that, within the context of standard displacement methods, the *return mapping algorithm (A22) is performed independently at each quadrature point of a typical element for a given total strain* ε_{n+1}. A global solution procedure based on Newton's method relies crucially on the use of consistent algorithmic tangent moduli $\mathbf{C}_{n+1}^{\text{ep}}$ introduced in Simo and Taylor,[15] and obtained by linearization of the return map. At each quadrature point one has the incremental relation

$$
\Delta\sigma_{n+1} = \mathbf{C}_{n+1}^{\text{ep}}\,\Delta\varepsilon_{n+1}
\tag{A23}
$$

where $\Delta\sigma_{n+1}$ and $\Delta\varepsilon_{n+1}$ are the stress and strain increments (at the quadrature point). As an example we consider *perfect plasticity* ($\mathbf{q} \equiv 0$). Define the tensor of moduli

$$
\Xi_{n+1} := [\mathbf{C}^{-1} + \Delta\gamma\partial^2\phi(\sigma_{n+1})/\partial\sigma_{n+1}^2]^{-1}
\tag{A24}
$$

and set for convenience $\nabla\phi_{n+1} := \partial\phi(\sigma_{n+1})/\partial\sigma_{n+1}$. Then, for $\phi_{n+1}^{\text{trial}} > 0$ (plastic loading) one finds the following expression,

$$
\mathbf{C}_{n+1}^{\text{ep}} = \Xi_{n+1} - \frac{\Xi_{n+1}\nabla\phi_{n+1} \otimes \Xi_{n+1}\nabla\phi_{n+1}}{\nabla\phi_{n+1}\cdot\Xi_{n+1}\nabla\phi_{n+1}}
\tag{A25}
$$

whereas $\mathbf{C}_{n+1}^{\text{ep}} = \mathbf{C}$ for $\phi_{n+1}^{\text{trial}} < 0$ (elastic loading).

2. Solution procedure

The finite element equations to be solved can be recast in a form entirely analogous to (22). To this end, define the strain field

$$
\boxed{\varepsilon_{n+1} = \mathbf{B}(\xi)\,\mathbf{d}_{n+1} + \mathbf{G}(\xi)\,\alpha_{n+1}}
\tag{A26}
$$

and regard the parameters α_{n+1} as element degrees of freedom, stored at the element level, but otherwise entirely analogous to the degrees of freedom $\mathbf{d}_{n+1}$.

Now define σ_{n+1} by the return map equations (A21)–(A22), and replace (23) by

$$
\left.
\begin{aligned}
\mathbf{f}_{e_{n+1}}^{\text{int}} &:= \int_{\mathscr{A}_e} \mathbf{B}^{\text{T}}\sigma_{n+1}\,\mathrm{d}V \\[6pt]
\mathbf{h}_{e_{n+1}} &:= \int_{\mathscr{A}_e} \mathbf{G}^{\text{T}}\sigma_{n+1}\,\mathrm{d}V = 0, \quad (e = 1, \ldots, n_{\text{elm}})
\end{aligned}
\right\}
\tag{A27}
$$

Observe that, for $\Delta\gamma \equiv 0$ in $\mathcal{B}_e$, these equations are identical to (23) except for the presence of the plastic strain ε_n^p. The solution of (A24) is performed iteratively (in a fashion similar to Section 2.2.3) using the following algorithm:

a. UPDATE nodal displacements at iteration $k + 1$:

$$\mathbf{d}^{(k+1)} = \mathbf{d}^{(k)} + \Delta\mathbf{d}^{(k)}$$

b. UPDATE[†] at the element level $\boldsymbol{\alpha}_e^{(k)}$ by setting

$$\boldsymbol{\alpha}_e^{(k+1)} = \boldsymbol{\alpha}_e^{(k)} - [\mathbf{H}_e^{(k)}]^{-1}[\boldsymbol{\Gamma}_e^{(k)}\Delta\mathbf{d}_e^{(k)} - \mathbf{h}_e^{(k)}]$$

c. COMPUTE total *enhanced* strain:

$$\tilde{\boldsymbol{\varepsilon}}^{(k+1)} = \mathbf{B}\mathbf{d}_e^{(k+1)} + \mathbf{G}\boldsymbol{\alpha}_e^{(k+1)}$$

d. COMPUTE $\boldsymbol{\sigma}_{n+1}^{(k+1)}$ and $\mathbf{C}_{n+1}^{ep^{(k+1)}}$ and update internal variables using a *standard strain driven return mapping* algorithm.

e. INTEGRATE element matrices and residuals:

$$\mathbf{H}_e^{(k+1)} := \int_{\mathcal{B}_e} \mathbf{G}^{\mathsf{T}}\mathbf{C}^{ep^{(k+1)}}\mathbf{G}\,\mathrm{d}V$$

$$\boldsymbol{\Gamma}_e^{(k+1)} := \int_{\mathcal{B}_e} \mathbf{G}^{\mathsf{T}}\mathbf{C}^{ep^{(k+1)}}\mathbf{B}\,\mathrm{d}V$$

$$\mathbf{k}_e^{(k+1)} := \int_{\mathcal{B}_e} \mathbf{B}^{\mathsf{T}}\mathbf{C}^{ep^{(k+1)}}\mathbf{B}\,\mathrm{d}V$$

$$\mathbf{h}_e^{(k+1)} := \int_{\mathcal{B}_e} \mathbf{G}^{\mathsf{T}}\boldsymbol{\sigma}_{n+1}^{(k+1)}\,\mathrm{d}V$$

$$\mathbf{f}_e^{int^{(k+1)}} := \int_{\mathcal{B}_e} \mathbf{B}^{\mathsf{T}}\boldsymbol{\sigma}_{n+1}^{(k+1)}\,\mathrm{d}V$$

f. COMPUTE modified internal load and tangent stiffness matrix by setting

$$\tilde{\mathbf{f}}_e^{int^{(k+1)}} = \tilde{\mathbf{f}}_e^{int^{(k+1)}} - [\mathbf{H}_e^{(k+1)}]^{-1}\mathbf{h}_e^{(k+1)}$$

$$\tilde{\mathbf{k}}_e^{(k+1)} = \mathbf{k}_e^{(k+1)} - [\boldsymbol{\Gamma}_e^{(k+1)}]^{\mathsf{T}}[\mathbf{H}_e^{(k+1)}]^{-1}[\boldsymbol{\Gamma}_e^{(k+1)}]$$

g. ASSEMBLE and SOLVE for a new nodal displacement increment

$$\tilde{R}^{(k+1)} := \mathop{\mathbf{A}}_{e=1}^{n_{elm}} [\mathbf{f}_e^{ext} - \tilde{\mathbf{f}}_e^{int}]$$

$$\tilde{\mathbf{K}}^{(k+1)} := \mathop{\mathbf{A}}_{e=1}^{n_{elm}} \tilde{\mathbf{k}}_e^{(k+1)}$$

$$\Delta\mathbf{d}^{(k+1)} := [\tilde{\mathbf{K}}^{(k+1)}]^{-1}\tilde{R}^{(k+1)}$$

h. SET $k \leftarrow k + 1$ GOTO a.

[†] The element residual $\mathbf{h}_e^{(k)}$ and the matrices $\mathbf{H}_e^{(k)}$ and $\boldsymbol{\Gamma}_e^{(k)}$ are stored from the previous iteration along with the parameters $\boldsymbol{\alpha}_e^{(k)}$

Convergence of the preceding algorithm, obtained by straightforward linearization of equations (22)–(23), is attained when $\| \tilde{\boldsymbol{R}}^{(k)} \| < \text{TOL}$.

REFERENCES

1. K. J. Bathe and F. Brezzi, 'A simplified analysis of two plate bending elements—The MITC4 and MITC9 elements', *Proc. Conference NUMETA 87*, University College of Swansea, Wales, July 1987.
2. K. J. Bathe and E. N. Dvorkin, 'A continuum mechanics based four-node shell element for general non-linear analysis', *Int. J. Comp. Aided Eng. Software*, 1 (1984).
3. G. P. Bazely, Y. K. Cheung, B. M. Irons and O. C. Zienkiewicz, 'Triangular elements in plate bending—Conforming and nonconforming solutions', *Proc. First Conference on Matrix Methods in Structural Mechanics*, Wright-Patterson ATBFB, Ohio, 1965.
4. T. Belytschko and W. E. Bachrach, 'Efficient implementation of quadrilaterals with high coarse-mesh accuracy', *Comp. Methods Appl. Mech. Eng.*, 23, 323–331 (1986).
5. P. G. Ciarlet, *The Finite Element Method for Elliptic Problems*, North-Holland, Amsterdam, 1978.
6. T. J. R. Hughes, 'Generalization of selective integration procedures to anisotropic and nonlinear media', *Int. j. numer. methods eng.*, 15, 1413–1418 (1980).
7. T. J. R. Hughes, *The Finite Element Method*, Prentice-Hall, Englewood Cliffs, New Jersey, 1987.
8. T. J. R. Hughes and T. E. Tezduyar, 'Finite elements based upon Mindlin plate theory with particular reference to the four-node bilinear isoparametric element', *J. Appl. Mech. ASME*, 587–596 (1981).
9. R. D. Kreig and S. W. Key, 'Implementation of a time dependent plasticity theory into structural computer programs', in J. A. Stricklin and K. J. Saczlski (eds.), *Constitutive Equations in Viscoplasticity: Computational and Engineering Aspects*, AMD-20, ASME, New York, 1976.
10. J. C. Nagtegaal, D. M. Parks and J. R. Rice, 'On numerically accurate finite element solutions in the fully plastic range', *Comp. Methods Appl. Mech. Eng.*, 4, 153–177 (1974).
11. T. H. H. Pian and K. Sumihara, 'Rational approach for assumed stress finite elements', *Int. j. numer. methods eng.*, 20, 1685–1695 (1985).
12. E. F. Puch and S. N. Atluri, 'Development and testing of stable, invariant, isoparametric curvilinear 2- and 3-D hybrid-stress elements', *Comp. Methods Appl. Mech. Eng.*, 47, 331–356 (1984).
13. J. C. Simo and T. J. R. Hughes, 'On the variational foundations of assumed strain methods', *J. Appl. Mech., ASME*, 53, 51–54 (1986).
14. J. C. Simo and T. J. R. Hughes, *Plasticity, Viscoplasticity and Viscoelasticity: Formulation, Algorithms and Numerical Analysis*, Springer-Verlag, Berlin, to appear.
15. J. C. Simo and R. L. Taylor, 'Consistent tangent operators for rate independent elasto-plasticity', *Comp. Methods Appl. Mech. Eng.*, 48, 101–118 (1985).
16. J. C. Simo and R. L. Taylor, 'A return mapping algorithm for plane stress elastoplasticity', *Int. j. numer. methods eng.*, 22, 649–670 (1986).
17. J. C. Simo, J. G. Kennedy and S. Govindjee, 'Non-smooth multisurface plasticity and viscoplasticity. Loading/unloading conditions and numerical algorithms', *Int. j. numer. methods eng.*, 26, 2161–2185 (1988).
18. J. C. Simo, J. G. Kennedy and R. L. Taylor, 'Complementary mixed finite element formulations of elastoplasticity', *Comp. Methods Appl. Mech. Eng.*, to appear.
19. J. C. Simo, R. L. Taylor and K. S. Pister, 'Variational and projection methods for the volume constraint in finite deformation elastoplasticity', *Comp. Methods Appl. Mech. Eng.*, 51, 177–208 (1985).
20. G. Strang and G. Fix, *An Analysis of the Finite Element Method*, Prentice-Hall, Englewood Cliffs, New Jersey, 1973.
21. R. L. Taylor, [1989], Private Communication, Aug. 1989.
22. R. L. Taylor, P. J. Beresford and E. L. Wilson, 'A non-conforming element for stress analysis', *Int. j. numer. methods eng.*, 10, 1211–1219 (1976).
23. R. L. Taylor, J. C. Simo, O. C. Zienkiewicz and A. C. Chan, 'The patch test: A condition for assessing finite element convergence', *Int. j. numer. methods eng.*, 22, 39–62 (1986).
24. M. L. Wilkins, 'Calculation of elastic–plastic flow', in B. Alder *et al.* (eds.), *Methods of Computational Physics 3*, Academic Press, New York, 1964.
25. E. L. Wilson, R. L. Taylor, W. P. Doherty and J. Ghaboussi, 'Incompatible displacement models', in S. J. Fenves *et al.* (eds.), *Numerical and Computer Models in Structural Mechanics*, Academic Press, New York, 1973.
26. O. C. Zienkiewicz, [1977], *The Finite Element Method*, 3rd edn, McGraw-Hill, London, 1977.
27. O. C. Zienkiewicz and R. L. Taylor, *The Finite Element Method, Vol. 1*, 4th edn, McGraw-Hill, London, 1989.
28. K. J. Willan, 'Finite element analysis of cellular structures', Ph.D. thesis at University of California, Berkeley.